Weierstraß-Institut

für Angewandte Analysis und Stochastik

Leibniz-Institut im Forschungsverbund Berlin e. V.

Preprint ISSN 2198-5855

Near-field imaging of obstacles with the factorization method: Fluid-solid interaction

Tao Yin[1], Guanghui Hu[2], Liwei Xu[3], Bo Zhang[4]

submitted: February 8, 2016

[1] College of Mathematics and Statistics
Chongqing University
China
E-Mail: taoyin_cqu@163.com

[2] Weierstrass Institute
Mohrenstr. 39
10117 Berlin
Germany
E-Mail: guanghui.hu@wias-berlin.de

[3] College of Mathematics and Statistics
Institute of Computing and Data Sciences
Chongqing University
China
E-Mail: xul@cqu.edu.cn

[4] LSEC and Institute of Applied Mathematics
AMSS
Chinese Academy of Sciences
Beijing 100190
China
E-Mail: b.zhang@amt.ac.cn

No. 2224

Berlin 2016

2010 *Mathematics Subject Classification.* 35R30, 74B05, 78A46.

Key words and phrases. Inverse scattering, fluid-solid interaction problem, factorization method, Helmholtz equation, Navier equation, near-field imaging, outgoing-to-incoming operator.

The work of T. Yin is partially supported by the China Scholarship Council and the NNSFC grants 11371385 and 11201506. The work of G. Hu is financed by the German Research Foundation (DFG) under grant No. HU 2111/1-2. The work of L. Xu is partially supported by the NNSFC grant 11371385, the Start-up fund of Youth 1000 plan of China and that of Youth 100 plan of Chongqing University. The work of B. Zhang is partially supported by the NNSFC grants 61379093 and 91430102. The authors would like to thank A. Lechleiter and S. Peters from Bremen University and X. Liu and H. Zhang from Chinese Academy of Sciences for stimulating discussions.

Edited by
Weierstraß-Institut für Angewandte Analysis und Stochastik (WIAS)
Leibniz-Institut im Forschungsverbund Berlin e. V.
Mohrenstraße 39
10117 Berlin
Germany

Fax: +49 30 20372-303
E-Mail: preprint@wias-berlin.de
World Wide Web: http://www.wias-berlin.de/

Abstract

Consider a time-harmonic acoustic point source incident on a bounded isotropic linearly elastic body immersed in a homogeneous compressible inviscid fluid. This paper is concerned with the inverse fluid-solid interaction (FSI) problem of recovering the elastic body from near-field data generated by infinitely many incident point source waves at a fixed energy. The incident point sources and the receivers for recording scattered signals are both located on a non-spherical closed surface, on which an outgoing-to-incoming (OtI) operator is appropriately defined. We provide a theoretical justification of the factorization method for precisely characterizing the scatterer by utilizing the spectrum of the near-field operator. This generalizes the imaging scheme developed in [G. Hu, J. Yang, B. Zhang, H. Zhang, *Inverse Problems* **30** (2014): 095005] to the case when near-field data are measured on non-spherical surfaces. Numerical examples in 2D are demonstrated to show the validity and accuracy of the inversion algorithm, even if limited aperture data are available on one or several line segments.

1 Introduction

Consider a time-harmonic acoustic point source wave incident on a bounded elastic solid immersed in a homogeneous fluid (cf. Fig. 1, right). The wavelength of incidence is supposed to be comparable with the diameter of the elastic scatterer. Due to the external incident acoustic field, an elastic wave is generated inside the solid, while the incident acoustic wave is scattered back into the fluid and propagate into the infinity. This leads to the fluid-solid interaction (FSI) problem with the scattering interface separating the domains of acoustic and elastic waves. This paper is concerned with the inverse scattering problem of determining the shape and position of the elastic obstacle from near-field measurement data. Such inverse problem has many applications in underwater acoustics and ultrasonic non-destructive evaluation (see, e.g. [18] and references therein). For instance, in immersion testing, objects are always put in a tank of water in order to minimize the energy loss of the ultrasound beam transmitting from a transducer into a medium and vice versa. In ocean acoustics, sonar is a commonly used tool for tracking and detecting objects under the sea surface (see Figure 1, left).

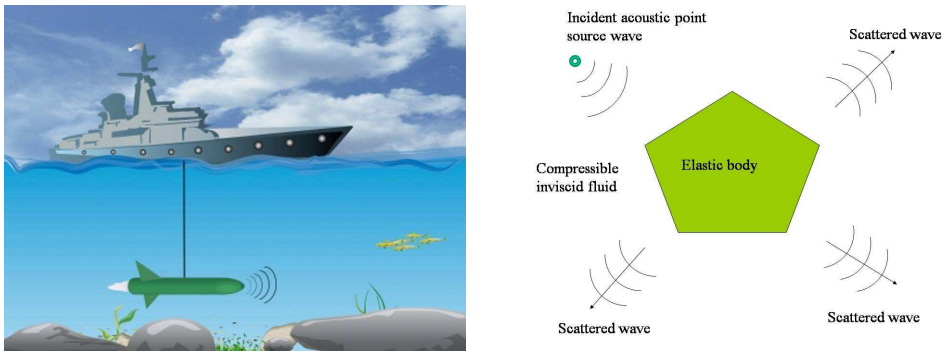

Figure 1: Right: the interaction problem between acoustic and elastic waves. Left: underwater research with a sonar submarine (source: http://www.freedigitalphotos.net/).

In this paper, the unknown obstacle is detected by sending infinitely many time-harmonic acoustic point sources at a fixed energy. The sources and receivers are supposed to be located on a non-spherical closed surface. We shall establish the factorization method of Kirsch [10, 11] for precisely characterizing the region occupied by the scatterer in terms of the spectrum of the near-field operator. As a sampling-type inversion scheme, the factorization method requires neither computation of direct solutions nor initial guesses. It provides a sufficient and necessary condition for recovering the shape and location of an obstacle (see Theorem 3.14), which can also be used as an efficient computational criterion. The original version of the factorization method was designed for inverse scattering of plane waves with infinitely many incident directions. We refer to the monograph [11] and references therein for a detailed discussion of the various versions of inverse acoustic scattering from impenetrable and penetrable scatterers. However, it is an open problem how to analyze the near-field operator within the same functional framework as in the far-field case until the recent study of the outgoing-to-incoming (OtI) operator carried out in [5]. The factorization scheme for treating the far-field operator does not extend to the near-field case since the resulting adjoint would be defined via a bilinear other than sesquilinear form, leading to essential difficulties in the characterization of the scatterer (see [11, Chapter 1.7] for details). A few approaches have been proposed so far, e.g., converting the near-field data to far-field patterns [11] (see also Section 4.2), constructing non-physical auxiliary operators [17] for connecting outgoing and incoming waves, or making use of non-physical incident point sources [13]. In [5], an OtI operator for the Helmholtz equation was constructed on a sphere for facilitating the factorization of the near-field operator, which can be more efficiently implemented than the earlier approaches. The scheme proposed in [5] seems promising for spherical measurement surfaces since the OtI mapping takes a simple form and is capable of recovering both impenetrable and penetrable acoustic scatterers.

The aim of this paper is to generalize the idea of [5] to the case of non-spherical measurement surfaces. In contrast to the simple form given in [5], the OtI mapping considered in this paper cannot be represented explicitly. Hence, difficulties arise from how to appropriately define and then discretize the OtI mapping when the measurement surface is not spherical; see Sections 3.3 and 4.1 for details. Our arguments have generalized the concept of the OtI operator defined on spheres. We also illustrate properties of the OtI mapping and its adjoint operator, which turns out to be an incoming-to-outgoing (ItO) mapping. We believe that one can mathematically justify a modified Linear Sampling Method [16] with near-field data in a rigorous way, as done in the far-field case shown in [12, Theorem 2.7]. As an application of the OtI operator, we investigate the inverse fluid-solid interaction problem by analyzing the product of the OtI and near-field operators. This product operator plays the analogous role of the far-field operator (see the

discussions at the end of Section 3.3), and has been used recently in [7] for determining the Dirichlet eigenvalues of the region occupied by a sound-soft obstacle from near-field measurements. Numerics show that our inversion scheme is more stable and efficient than the approach of converting near-field data to far-field patterns. Particularly, it is numerically applicable even if limited aperture data are available only. In our numerical experiments, the measurement curve in 2D is allowed to be a (finite) line segment, which might have important applications in non-destruction testing with line-array transducers.

Other imaging schemes for inverse FSI interaction can be found in [2, 3] where an optimization-based technique is applied and in [15, 16] using the reciprocity gap (RG) and linear sampling methods (LSM). The factorization method established in [12] involves far-field patterns corresponding to infinitely many incident plane waves, but without numerical tests. In this paper, the definition of the middle operator slightly differs from that of [12], but shows convenience in simplifying our arguments (cf. Lemma 3.11 and [12]). The proof of the denseness and compactness of the near-field solution operator is more involved than [12]; see Section 3.2.

In the subsequent Section 2, we rigorously formulate the direct and inverse FSI interaction problems. Section 3 is devoted to the theoretical justification of the factorization method using near-field measurement data. The OtI mapping and its adjoint will be introduced and investigated in Section 3.3, and the inversion scheme will be stated in Section 3.5. Discretization schemes and a number of numerical experiments are reported in Section 4.

2 Direct and inverse interaction problems

We formulate the fluid-solid interaction (FSI) problem following [4, 14]. Let $\Omega \subset \mathbb{R}^3$ be a bounded domain with the C^2-smooth boundary Γ and denote by ν the unit normal vector to Γ directed into the exterior of Ω. We assume that Ω is occupied by an isotropic linearly elastic solid characterized by the real-valued constant mass density $\rho > 0$ and the Lamé constants $\lambda, \mu \in \mathbb{R}$ satisfying $\mu > 0, 3\lambda + 2\mu > 0$. The exterior $\Omega^c := \mathbb{R}^3 \backslash \overline{\Omega}$, which is assumed to be connected, is filled with a homogeneous compressible inviscid fluid with the constant mass density $\rho_f > 0$. Let $k = \omega/c > 0$ be the wave number in the fluid, where $\omega > 0$ denotes the frequency of the time harmonic incoming wave and $c > 0$ the sound speed. Let p^i be a point source of the form

$$p^i(x) = p^i(x, z) = \Phi_k(x, z), \quad x \in \mathbb{R}^3, \quad z \in \mathbb{R}^3 \backslash \overline{\Omega}, \quad x \neq z, \tag{1}$$

where $\Phi_k(x, z)$ is the free space fundamental solution of the Helmholtz equation in $\mathbb{R}^3$ with wave number k, that is,

$$\Phi_k(x, z) = \frac{e^{ik|x-z|}}{4\pi|x - z|}, \qquad x, z \in \mathbb{R}^3, \quad x \neq z. \tag{2}$$

Due to the external incidence, an outgoing acoustic wave p^s is scattered back into the fluid propagating into the infinity, while an elastic wave $u = (u_1, u_2, u_3)^\top$ is incited inside Ω. Under the hypothesis of small amplitude oscillations in both the solid and the fluid, the direct or forward scattering problem can be formulated as the following boundary value problem (see, e.g., [4, 14, 18]): determine $u \in H^1(\Omega)^3$ and

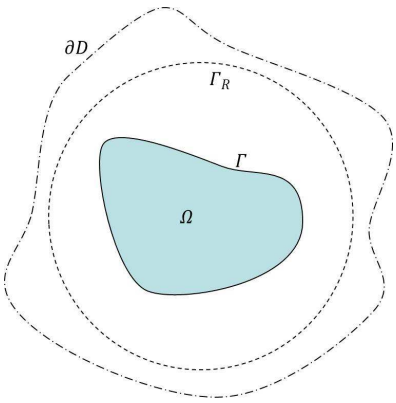

Figure 2: The geometric setting of our scattering problem: Ω denotes the elastic body, $\partial D := \{x \in \mathbb{R}^3 : x = \hat{x}\,\gamma(\hat{x})\}$ is the (non-spherical) surface where incident point sources are located and near-field data are measured.

the total acoustic field $p \in H^1_{loc}(\Omega^c \backslash \{z\})$ such that

$$\Delta^* u + \rho\omega^2 u = 0 \quad \text{in} \quad \Omega, \quad \Delta^* := \mu\Delta + (\lambda+\mu)\,\nabla\nabla\cdot\,, \tag{3}$$

$$\Delta p + k^2 p = 0 \quad \text{in} \quad \Omega^c \backslash \{z\}, \tag{4}$$

$$\eta\, u\cdot\nu = \partial_\nu p \quad \text{on} \quad \Gamma, \quad \eta = \rho_f\omega^2 > 0, \tag{5}$$

$$\mathbf{T}\, u = -\nu p \quad \text{on} \quad \Gamma. \tag{6}$$

Here, $\partial_\nu p = \nu\cdot\nabla p$ denotes the normal derivative of p on Γ and $\mathbf{T}$ stands for the standard stress operator defined by

$$\mathbf{T}\, u = 2\mu\,\partial_\nu u + \lambda\nu\,(\nabla\cdot u) + \mu\,\nu\times(\nabla\times u) \quad \text{on} \quad \Gamma. \tag{7}$$

Furthermore, the scattered field $p^s = p - p^i$ satisfies the Sommerfeld radiation condition

$$\lim_{r\to\infty} r\Big(\frac{\partial p^s}{\partial r} - ikp^s\Big) = 0, \quad r = |x|, \tag{8}$$

which holds uniformly in $\hat{x} = x/|x| \in \mathbb{S}^2 := \{\hat{\theta}\in\mathbb{R}^3 : |\hat{\theta}| = 1\}$. From this radiation condition it follows that the scattered field p^s has the asymptotic behavior of an outgoing spherical wave

$$p^s(x) = \frac{e^{ik|x|}}{4\pi|x|}\left\{p^\infty(\hat{x}) + O\left(\frac{1}{|x|}\right)\right\} \quad \text{as} \quad |x|\to\infty \tag{9}$$

uniformly in all directions $\hat{x}$, where $p^\infty(\hat{x})$ defined on the unit sphere $\mathbb{S}^2$ is known as the far field pattern of the scattered field with the argument $\hat{x}$ denoting the observation direction.

Throughout the paper it is supposed that ω is not a Jones frequency, so that the problem (3)-(6) and (8) is always uniquely solvable (see, e.g., [8,9]). Notice that $\omega\in\mathbb{R}$ is called a Jones frequency if the boundary value problem

$$\Delta^* u_0 + \rho\omega^2 u_0 = 0 \quad \text{in} \quad \Omega, \qquad \mathbf{T}\, u_0 = 0, \quad u_0\cdot\nu = 0 \quad \text{on} \quad \Gamma,$$

admits a nontrivial solution. Furthermore, the transmission problem

$$\begin{aligned} \Delta^* u + \rho\omega^2 u &= 0 \quad \text{in} \quad \Omega, \\ \Delta p^s + k^2 p^s &= 0 \quad \text{in} \quad \Omega^c, \\ \eta u \cdot \nu - \partial_\nu p^s &= f \quad \text{on} \quad \Gamma, \\ \mathbf{T}\, u + \nu p^s &= h \quad \text{on} \quad \Gamma, \end{aligned}$$

with p^s satisfying the Sommerfeld radiation condition (8), has a unique solution $(p^s, u) \in H^1_{loc}(\Omega^c) \times H^1(\Omega)^3$ for all $f \in H^{-1/2}(\Gamma)$, $h \in H^{-1/2}(\Gamma)^3$ provided that ω is not a Jones frequency [15, Theorem 3.3]. Given an incident wave $p^i(\cdot, z)$ with $z \in \Omega^c$, we use $p^s(\cdot, z), p^\infty(\cdot, z)$ to indicate the dependence of the scattered field and far-field pattern on the source position z.

Set $B_R(y) := \{x \in \mathbb{R}^3 : |x - y| < R\}$, and for simplicity write $B_R = B_R(O)$ with the boundary $\Gamma_R = \{x : |x| = R\}$. In this paper we assume for simplicity that the incident point sources are located on the boundary of a star-shaped domain D containing Ω, that is, the boundary of D can be represented as

$$\partial D = \{x \in \mathbb{R}^3 : x = \hat{x}\, \gamma(\hat{x})\} \tag{10}$$

where $\gamma : \mathbb{S}^2 \to \mathbb{R}$ is a positive and continuous function. Moreover, we assume that the scattered data are also measured on ∂D, that $\Omega \subset B_R \subset D$ for some $R > 0$, and that k^2 is not the Dirichlet eigenvalue of $-\Delta$ over D. The inverse scattering problem under consideration is to determine the shape and location of the obstacle Ω from the near-field data $\{p^s(x, z) : x, z \in \partial D\}$ due to the point sources $p^i(\cdot, z)$ with $z \in \partial D$. The scattered fields $p^s(x, z)$ for all $x, z \in \partial D$ define the near-field operator $N : L^2(\partial D) \to L^2(\partial D)$ by

$$(N\varphi)(x) = \int_{\partial D} p^s(x, z)\, \varphi(z)\, ds(z) \quad \text{for} \quad x \in \partial D. \tag{11}$$

Clearly, $N\varphi$ is the restriction to ∂D of the scattered field generated by the incident wave

$$\int_{\partial D} p^i(x, z)\, \varphi(z)\, ds(z), \qquad x \in D.$$

Remark 2.1. In this paper, the measurement surface ∂D is assumed to be a star-shaped surface taking the form (10) and lying in $|x| > R$ for some $R > 0$. With these assumptions we can readily define and efficiently implement the OtI operator (see Section 3.3). A detailed description of the discretization schemes will be stated in Section 4.1. For non-star-shaped measurement surfaces, the OtI operator is still well-defined and can be computed, for instance, by solving second kind integral equations defined on ∂D. The reader is referred to (38) for the expression of the OtI operator in terms of the doubly-layer potential and its adjoint.

3 Factorization of near-field operator

In this section, we will establish a suitable factorization of the near-field operator N corresponding to incident point sources $p^i(\cdot, z) = \Phi_k(x, z)$ for all $z \in \partial D$. Compared to the far-field case, the essential ingredient in our analysis is to define the outgoing-to-incoming operator T so that the factorization form $TN = (TG)J^*(TG)^*$ holds, where J and G are referred to as the middle operator and solution operator to be defined later. Since the measurement surface is not necessarily spherical, our augment generalizes the approach developed in [5] which was valid only when ∂D is a sphere.

3.1 Auxiliary boundary value problems

We introduce several auxiliary boundary value problems for establishing the factorization method. For $h \in H^{1/2}(\Gamma)$, consider the boundary value problem of finding $w \in H^1(\Omega)$ such that

$$\Delta w + k^2 w = 0 \quad \text{in} \quad \Omega, \qquad w = h \quad \text{on} \quad \Gamma. \tag{12}$$

Suppose k^2 is not a Dirichlet eigenvalue of $-\Delta$ in Ω. Then, the above problem (12) is uniquely solvable and the normal derivative of w on Γ defines the interior Dirichlet-to-Neumann (DtN) map $\Lambda : H^{1/2}(\Gamma) \to H^{-1/2}(\Gamma)$ by $h \mapsto \partial_\nu w|_\Gamma$. Further, we have

Lemma 3.1. *Assume that k^2 is not a Dirichlet eigenvalue of $-\Delta$ in Ω. Then it holds that*

$$\int_\Gamma (\Lambda h)\, g\, ds = \int_\Gamma (\Lambda g)\, h\, ds \qquad \textit{for all} \quad h \in H^{1/2}(\Gamma),\ g \in H^{1/2}(\Gamma). \tag{13}$$

Proof. Let w and v be the unique solution to the problem (12) with the Dirichlet data h and g, respectively. Applying Green's formula yields

$$\int_\Gamma (\Lambda h)\, g\, ds - \int_\Gamma (\Lambda g)\, h\, ds = \int_\Gamma (\partial_\nu w\, v - \partial_\nu v\, w)\ ds = \int_\Omega (\Delta w\, v - \Delta v\, w)\ dx = 0.$$

□

Lemma 3.1 will be used to derive the adjoint of the solution operator in Section 3.2 below. With the definition of Λ, we introduce the second auxiliary boundary value problem as follows: Given $h \in H^{1/2}(\Gamma)$, find $u \in H^1(\Omega)^3$ and $p^s \in H^1_{loc}(\Omega^c)$ such that

$$\begin{aligned}
\Delta^* u + \rho\omega^2 u &= 0 \quad \text{in} \quad \Omega, && (14)\\
\Delta p^s + k^2 p^s &= 0 \quad \text{in} \quad \Omega^c, && (15)\\
\eta u \cdot \nu - \partial_\nu p^s &= \Lambda h \quad \text{on} \quad \Gamma, && (16)\\
\mathbf{T} u + \nu p^s &= -\nu h \quad \text{on} \quad \Gamma, && (17)
\end{aligned}$$

and that p^s satisfies the Sommerfeld radiation condition (8). Since ω is not a Jones frequency, there is a unique solution (u, p^s) to the problem (14)-(17). Clearly, our forward scattering problem can be equivalently formulated as the problem (14)-(17) with $h = p^i(\cdot, z)|_\Gamma$, since $\Lambda(p^i(\cdot, z)|_\Gamma) = \partial_\nu p^i(\cdot, z)|_\Gamma$ for all $z \in \Omega^c$.

To justify the factorization method, we need to consider the following interior boundary value problem: Find $u \in H^1(\Omega)^3$ and $w \in H^1(\Omega)$ such that

$$\begin{aligned}
\Delta^* u + \rho\omega^2 u &= 0 \quad \text{in} \quad \Omega, && (18)\\
\Delta w + k^2 w &= 0 \quad \text{in} \quad \Omega, && (19)\\
\eta u \cdot \nu - \partial_\nu w &= f \quad \text{on} \quad \Gamma, && (20)\\
\mathbf{T} u + \nu w &= g \quad \text{on} \quad \Gamma && (21)
\end{aligned}$$

with $f \in H^{-1/2}(\Gamma)$ and $g \in H^{-1/2}(\Gamma)^3$. We call ω an interior transmission eigenvalue if there exists a non-trivial solution pair $(w, u) \in H^1(\Omega) \times H^1(\Omega)^3$ to the homogeneous system (18)-(21) with $f = g = 0$. In [12], it was shown that the set of such eigenvalues is at most discrete with the only possible

accumulating point at infinity if $3\eta \neq (3\lambda + 2\mu)k^2$ and there exists $\delta > 0$ such that $\rho \geq \rho_f + \delta$. This leads to the existence and uniqueness of solutions to the problem (18)-(21) for all $\omega \in \mathbb{R}^+ \backslash \mathcal{D}$ with some discrete set $\mathcal{D}$. In particular, the mapping $(f, g) \to (w, u)$ in problem (18)-(21) is bounded from $H^{-1/2}(\Gamma) \times H^{-1/2}(\Gamma)^3$ to $H^1(\Omega) \times H^1(\Omega)^3$. Further, one can observe that, if v is a solution to (12) with $h \in H^{1/2}(\Gamma)$, then the solution $(w, u) = (v, 0)$ uniquely solves the problem (18)-(21) with $f = -(\partial_\nu v)|_\Gamma$ and $g = (\nu v)|_\Gamma$.

In the subsequent sections the problems (12), (14)-(17) and (18)-(21) are always supposed to be uniquely solvable with the incidence frequency under question.

3.2 Solution operator

The solution operator $G : H^{1/2}(\Gamma) \to L^2(\partial D)$ is defined as

$$G\, h = p^s|_{\partial D}, \tag{22}$$

where $p^s \in H^1_{loc}(\Omega^c)$ is the unique solution to the problem (14)-(17). An explicit expression of the adjoint of G is shown as below.

Lemma 3.2. *The explicit expression of $G^* : L^2(\partial D) \to H^{-1/2}(\Gamma)$ is given by*

$$G^* g = -\overline{[\rho_f \omega^2 \tilde{u} \cdot \nu + \Lambda(\boldsymbol{T}\tilde{u} \cdot \nu)]} \quad \textit{for} \quad g \in L^2(\partial D), \tag{23}$$

where $\tilde{u}$, together with some $\tilde{p}^s$, is the unique solution to (14)-(17) with

$$h(y) = q(y)|_\Gamma, \qquad q(y) := \int_{\partial D} \Phi_k(x, y)\, \overline{g}(x)\, ds(x) \quad \textit{for} \quad y \in \mathbb{R}^3. \tag{24}$$

Remark 3.3. Since $g \in L^2(\partial D)$, we know $h \in H^{3/2}(\Gamma) \subset H^{1/2}(\Gamma)$ and thus by (17), $\mathbf{T}\,\tilde{u} \cdot \nu = -(h + \tilde{p}^s) \in H^{1/2}(\Gamma)$ on Γ. Hence, the operator $G^* : L^2(\partial D) \to H^{-1/2}(\Gamma)$ defined by (23) is well-defined.

Proof. For $h \in H^{1/2}(\Gamma)$, let (u, p^s) be the solution of the problem (14)-(17). By the definition of G, we see

$$\langle G\, h, g \rangle_{L^2(\partial D)} = \int_{\partial D} p^s \overline{g}\, ds, \tag{25}$$

where $\langle \cdot, \cdot \rangle_{L^2(\partial D)}$ denotes the inner product in $L^2(\partial D)$. Recalling Green's second formula, we can represent p^s as

$$p^s(x) = \int_\Gamma \left[\partial_\nu \Phi_k(x, y)\, p^s(y) - \Phi_k(x, y)\, \partial_\nu p^s(y)\right] ds(y) \quad \text{for} \quad x \in \mathbb{R}^3 \backslash \overline{\Omega}.$$

Inserting the above expression into (25) and changing the order of integration yield

$$\langle G\, h, g \rangle_{L^2(\partial D)} = \int_\Gamma \left[\partial_\nu q\, p^s - q\, \partial_\nu p^s\right] ds, \tag{26}$$

where q is defined in (24). Let $(\tilde{u}, \tilde{p})$ be defined in Lemma 3.3. Then using the boundary conditions

$$\Lambda\, q = \eta\, (\tilde{u} \cdot \nu) - \partial_\nu \tilde{p}, \quad \nu q = -(\mathbf{T}\,\tilde{u} + \nu \tilde{p}),$$

it follows from (26) that

$$\langle G\,h, g\rangle_{L^2(\partial D)} = \int_\Gamma \left[\eta(\tilde{u}\cdot\nu)\,p^s - \partial_\nu\tilde{p}^s\,p^s\right]\,ds + \int_\Gamma \nu\cdot(\mathbf{T}\tilde{u} + \nu\tilde{p}^s)\,\partial_\nu p^s\,ds. \tag{27}$$

Since $\tilde{p}^s$ and p^s are both radiating solutions in Ω^c, we have that for any $R' > R$

$$\int_\Gamma \left[\partial_\nu\tilde{p}^s\,p^s - \tilde{p}^s\,\partial_\nu p^s\right]\,ds = \int_{\Gamma_{R'}} \left[\partial_\nu\tilde{p}^s\,p^s - \tilde{p}^s\,\partial_\nu p^s\right]\,ds \to 0$$

as $R' \to \infty$. Hence, by (27),

$$\langle G\,h, g\rangle_{L^2(\partial D)} = \int_\Gamma \left[(\mathbf{T}\tilde{u}\cdot\nu)\,\partial_\nu p^s + \eta\,(\tilde{u}\cdot\nu)\,p^s\right]\,ds.$$

Recalling the coupling conditions

$$\partial_\nu p^s = \eta u\cdot\nu - \Lambda\,h, \quad \nu p^s = -(\mathbf{T}\,u + \nu\,h)$$

we arrive at the identity

$$\langle G\,h, g\rangle_{L^2(\partial D)} = -\int_\Gamma h\,[\eta\,\tilde{u}\cdot\nu + \Lambda(\mathbf{T}\,\tilde{u}\cdot\nu)]\,ds, \tag{28}$$

where we have used Lemma 3.1 and the relation

$$\int_\Gamma (\mathbf{T}\,\tilde{u}\cdot u - \mathbf{T}\,u\cdot\tilde{u})\,ds = 0$$

which can be proved by Betti's formula. The expression of G^* then follows directly from (28). □

The representation of G^* can be used to verify the denseness of Range(G) in $L^2(\partial D)$; see Lemma 3.4 below. We refer to [15] for the proof of the compactness and denseness of the far-field solution operator corresponding to incident plane waves.

Lemma 3.4. *The solution operator $G : H^{1/2}(\Gamma) \to L^2(\partial D)$ is compact with a dense range in $L^2(\partial D)$.*

Proof. For $h \in H^{1/2}(\Gamma)$, let (u, p^s) be the unique solution to problem (14)-(17). Then

$$\|G\,h\|_{L^2(\partial D)} = \|p^s\|_{L^2(\partial D)} \le \|p^s\|_{H^{1/2}(\partial D)} \le c\,\|h\|_{H^{1/2}(\Gamma)}, \quad c > 0,$$

where the last inequality is a consequence of the stability estimate for the auxiliary boundary value problem (14)-(17). The compactness of G then follows immediately from the decomposition $G = G_2G_1$, where G_1, defined as $G_1h = p^s|_{\partial D}$, is a bounded map from $H^{1/2}(\Gamma)$ to $H^{1/2}(\partial D)$ and $G_2 : H^{1/2}(\partial D) \to L^2(\partial D)$ is compact.

To prove the denseness of G, it suffices to verify the injectivity of $G^* : L^2(\partial D) \to H^{-1/2}(\Gamma)$. Suppose now $G^*g = 0$ and let $\tilde{u}, \tilde{p}^s$ and q be specified as in Lemma 3.2. By Lemma 3.2, the relation $\eta\tilde{u}\cdot\nu + \Lambda(\mathbf{T}\,\tilde{u}\cdot\nu) = 0$ holds on Γ. This, together with the coupling boundary conditions between $\tilde{u}$ and $\tilde{p}^s$, implies that

$$\partial_\nu\tilde{p}^s = -\Lambda(\mathbf{T}\tilde{u}\cdot\nu + q|_\Gamma), \quad \tilde{p}^s = -(\mathbf{T}\tilde{u}\cdot\nu + q|_\Gamma) \quad \text{on} \quad \Gamma. \tag{29}$$

Let $\tilde{Q}$ be the solution of problem (12) with $h = -(\mathbf{T}\,\tilde{u}\cdot\nu + q)|_\Gamma \in H^{1/2}(\Gamma)$. Define

$$Q := \tilde{Q} \quad \text{in} \quad \Omega, \quad Q := \tilde{p}^s \quad \text{in} \quad \mathbb{R}^3\backslash\overline{\Omega}.$$

The relation (29) and the definition of Λ imply that

$$Q^- = Q^+, \quad \partial_\nu Q^- = \partial_\nu Q^+ \quad \text{on} \quad \Gamma,$$

where the superscripts '-' and '+' denote respectively the limits from inside and outside Ω. Thus Q is an entire radiating solution of the Helmholtz equation in the whole space, implying that $Q = 0$ in $\mathbb{R}^3$. In particular, $\tilde{p}^s = Q \equiv 0$ in $\mathbb{R}^3\backslash\overline{\Omega}$ and thus $\tilde{p}^s = \partial_\nu \tilde{p}^s = 0$ on Γ. Consequently, by (29),

$$\partial_\nu q = -\Lambda(\mathbf{T}\tilde{u}\cdot\nu) = \eta\,(\tilde{u}\cdot\nu), \quad q = -\mathbf{T}\tilde{u}\cdot\nu \quad \text{on} \quad \Gamma.$$

This suggests that the solution pair $(\tilde{u}, q)$ is the unique solution to the homogeneous problem (18)-(21) with $f = g = 0$. By uniqueness it holds that $q = 0$ in Ω, and by the unique continuation $q = 0$ in D. Hence we get $q = 0$ on ∂D and $q = 0$ in $\mathbb{R}^3\backslash\overline{D}$ due to the uniqueness of solutions to the exterior boundary value problem of the Helmholtz equation in $\mathbb{R}^3\backslash\overline{D}$. Finally, we obtain $g = 0$ on ∂D as a consequence of the jump relation $\overline{g} = \partial_\nu q^- - \partial_\nu q^+$ on ∂D. This completes the proof. □

3.3 Outgoing-to-Incoming (OtI) mapping

In this subsection we give a precise definition of the OtI operator on non-spherical surfaces. Let Y_n^m be the normalized spherical harmonic functions of order n,

$$Y_n^m(\theta,\phi) = \sqrt{\frac{2n+1}{4\pi}\frac{n-|m|}{n+|m|}}P_n^{|m|}(\cos\theta)e^{im\phi}, \quad n = 0,1,2,\cdots, \quad m = -n,\cdots,n,$$

where (θ,ϕ) represents the spherical coordinates on the unit sphere and P_n^m are the *associated Legendre functions*. Let j_n and $h_n^{(1)}$ be the spherical Bessel functions and spherical Hankel functions of order n, respectively.

Definition 3.5. *Let G be the solution operator and assume that $f \in$ Range(G), that is, $f = p^s|_{\partial D}$, where $p^s \in H^1_{loc}(\Omega^c)$ is the unique radiation solution to the problem (14)-(17) with some $h \in H^{1/2}(\Gamma)$. Suppose p^s admits the expansion*

$$p^s(x) = \sum_{n=0}^{\infty}\sum_{m=-n}^{n} p_{n,m}\, h_n^{(1)}(k|x|)Y_n^m(\hat{x}), \quad p_{n,m} \in \mathbb{C}, \quad \textit{in} \quad |x| \geq R.$$

Then the outgoing-to-incoming mapping T : Range$(G) \to L^2(\partial D)$ is defined as $Tf = \tilde{p}^s|_{\partial D}$, with

$$\tilde{p}^s(x) = -\sum_{n=0}^{\infty}\sum_{m=-n}^{n} p_{n,m}\,\overline{h_n^{(1)}(k|x|)}\,Y_n^m(\hat{x}), \quad x \in \Omega^c. \tag{30}$$

By definition, the mapping $T : H^{1/2}(\partial D) \to L^2(\partial D)$ is linear, bounded and one-to-one. Since the domain Range(G) of T is dense in $L^2(\partial D)$ (see Lemma 3.4), T can be extended to a linear, bounded and one-to-one operator mapping $L^2(\partial D)$ into itself, which, for simplicity, is denoted again by T. The next result summarizes some properties of $T : L^2(\partial D) \to L^2(\partial D)$.

Lemma 3.6. **(i)** $T(\Phi_k(\cdot,z)|_{\partial D}) = \overline{\Phi_k(\cdot,z)}|_{\partial D}$ *for* $z \in \Omega$.

(ii) T *has a dense range in* $L^2(\partial D)$.

(iii) *Assume that* $T(p^s|_{\partial D}) = \tilde{p}^s|_{\partial D}$, *where* p^s *and* $\tilde{p}^s$ *are outgoing and incoming solutions to the Helmholtz equation in* Ω^c, *respectively. Then* $\tilde{p}^s$ *has the asymptotic behavior*

$$\tilde{p}^s(x) = \frac{e^{-ik|x|}}{4\pi|x|}\left\{p^\infty(-\hat{x}) + O\left(\frac{1}{|x|}\right)\right\} \quad \text{as} \quad |x| \to \infty. \tag{31}$$

Here p^∞ *denotes the far-field pattern of the outgoing radiating solution* p^s.

Proof. (i) Let $f := \Phi_k(\cdot,z)|_{\partial D}$ and assume that $p^s \in H^1_{loc}(\Omega^c)$ is the radiating solution to the problem (14)-(17) such that $p^s|_{\partial D} = f$. By uniqueness, $p^s = \Phi_k(\cdot,z)$ in Ω^c for any fixed $z \in \Omega$. Recall the *addition theorem* for the fundamental solution

$$\Phi_k(x,z) = ik\sum_{n=0}^{\infty}\sum_{m=-n}^{n} h_n^{(1)}(k|x|)\, Y_n^m(\hat{x})\, j_n(k|z|)\, \overline{Y_n^m(\hat{z})} \quad \text{for} \quad |x| > R, z \in \Omega. \tag{32}$$

Using the relation $Y_n^m = \overline{Y_n^{-m}}$, we obtain

$$\begin{aligned}\overline{\Phi_k(x,z)} &= -ik\sum_{n=0}^{\infty}\sum_{m=-n}^{n} \overline{h_n^{(1)}(k|x|)}\; \overline{Y_n^m(\hat{x})} j_n(k|z|)\, Y_n^m(\hat{z}) \\ &= -ik\sum_{n=0}^{\infty}\sum_{m=-n}^{n} \overline{h_n^{(1)}(k|x|)}\; Y_n^m(\hat{x}) j_n(k|z|)\, \overline{Y_n^m(\hat{z})}. \end{aligned} \tag{33}$$

The first assertion then follows from (32), (33) and the definition of T.

(ii) Since k^2 is not a Dirichlet eigenvalue of $-\Delta$ in D, one can readily prove that the set $\{\overline{\Phi_k(\cdot,z)}|_{\partial D} : z \in \Omega\}$ is dense in $L^2(\partial D)$. Therefore, the denseness of Range(G) follows directly from the first assertion.

(iii) Suppose p^s and $\tilde{p}^s$ are expanded as those in Definition 3.5. From the asymptotic behavior of the Hankel functions with a large argument we know

$$p^\infty(\hat{x}) = \frac{1}{k}\sum_{n=0}^{\infty}\frac{1}{i^{n+1}}\sum_{m=-n}^{n} p_{n,m}\, Y_n^m(\hat{x})$$

On the other hand, the incoming solution $\tilde{p}^s$ has the asymptotic behavior

$$\tilde{p}^s(x) = \frac{e^{-ik|x|}}{4\pi|x|}\left\{\tilde{p}^\infty(\hat{x}) + O\left(\frac{1}{|x|}\right)\right\} \quad \text{as} \quad |x| \to \infty,$$

with

$$\tilde{p}^\infty(\hat{x}) = -\frac{1}{k}\sum_{n=0}^{\infty}\frac{(-1)^{n+1}}{i^{n+1}}\sum_{m=-n}^{n} p_{n,m}\, Y_n^m(\hat{x}).$$

Making use of the relation

$$Y_n^m(\hat{x}) = (-1)^n\, Y_n^m(-\hat{x}),$$

we obtain $\tilde{p}^\infty(\hat{x}) = p^\infty(-\hat{x})$, which completes the proof of the third assertion. □

If the measurement surface $\partial D = \{x : |x| = R_1\}$ is a sphere with the radius $R_1 > R$, the outgoing-to-incoming mapping T takes the following explicit form (see [5]):

$$(Tg)(x) = \int_{\Gamma_{R_1}} K(x,y)\, g(y)\, ds(y) \quad \text{for} \quad g \in L^2(\Gamma_{R_1}) \tag{34}$$

with the kernel

$$K(x,y) := -\frac{1}{4\pi R_1^2} \sum_{n=0}^{\infty} \left(\frac{\overline{h_n^{(1)}(kR_1)}}{h_n^{(1)}(kR_1)} \right) (2n+1) P_n(\cos\theta). \tag{35}$$

In (35), P_n are the Legendre polynomials and θ denotes the angle between $x, y \in \Gamma_{R_1}$. The derivation of (34) was based on the expansion of g in terms of its Fourier coefficients on $|x| = R_1$. The analogous form of (34) for non-spherical ∂D will be derived in Section 4.1. In the following we propose another numerical scheme to implement T.

Given $f \in \text{Range}(G)$, we assume that $f = p^s|_{\partial D} \in L^2(\partial D)$, where $p^s \in H^1_{loc}(\Omega^c)$ is some radiating solution to the problem (14)-(17). We make an ansatz on the solution as follows:

$$p^s(x) = \int_{\partial D} \frac{\partial \Phi^{(k)}(x,y)}{\partial \nu(y)} \varphi(y)\, ds(y), \qquad x \in D^c := \mathbb{R}^3 \backslash \overline{D}, \tag{36}$$

where $\varphi \in L^2(\partial D)$ is the unique solution of the second kind integral equation

$$(\frac{1}{2}\mathbf{I} + \mathcal{D})\, \varphi = p^s|_{\partial D} = f \quad \text{on} \quad \partial D,$$

with

$$(\mathcal{D}\varphi)(x) := \int_{\partial D} \frac{\partial \Phi^{(k)}(x,y)}{\partial \nu(y)} \varphi(y)\, ds(y), \quad x \in \partial D.$$

Clearly, the adjoint operator of $\mathcal{D}$ in $L^2(\partial D)$ is given by

$$(\mathcal{D}^*\varphi)(x) := \int_{\partial D} \frac{\partial \overline{\Phi^{(k)}(x,y)}}{\partial \nu(y)} \varphi(y)\, ds(y), \quad x \in \partial D.$$

By Lemma 3.5 (i), the incoming solution $\tilde{p}^s$ corresponding to p^s should be of the form

$$\tilde{p}^s(x) = \int_{\partial D} \frac{\partial \overline{\Phi^{(k)}(x,y)}}{\partial \nu(y)} \varphi(y)\, ds(y), \qquad x \in D^c := \mathbb{R}^3 \backslash \overline{D}. \tag{37}$$

The definition of T together with the jump relation of the double-layer potential gives

$$Tf = (\frac{1}{2}\mathbf{I} + \mathcal{D}^*)\, \varphi = (\frac{1}{2}\mathbf{I} + \mathcal{D}^*)\, (\frac{1}{2}\mathbf{I} + \mathcal{D})^{-1}\, f \quad \text{for all} \quad f \in \text{Range}(G).$$

By the denseness of $\text{Range}(G)$ in $L^2(\partial D)$, we obtain

$$T = (\frac{1}{2}\mathbf{I} + \mathcal{D}^*)\, (\frac{1}{2}\mathbf{I} + \mathcal{D})^{-1} : \quad L^2(\partial D) \to L^2(\partial D). \tag{38}$$

Hence, the adjoint operator T^* takes the form

$$T^* = (\frac{1}{2}\mathbf{I} + \mathcal{D}^*)^{-1} (\frac{1}{2}\mathbf{I} + \mathcal{D}) \; : \quad L^2(\partial D) \to L^2(\partial D). \tag{39}$$

Remark 3.7. (i) Obviously, the implementation of the outgoing-to-incoming mapping T depends on the surface ∂D only. The computation of $(\frac{1}{2}\mathbf{I}+\mathcal{D})^{-1}$ in (38) is amount to solving an exterior boundary value problem in D^c. Alternatively, we may express the solution p^s as a single-layer potential, leading to the relation

$$T\left(\int_\Gamma \Phi^{(k)}(x,y)\,\varphi(y)\,ds(y)\right)=\int_\Gamma \overline{\Phi^{(k)}(x,y)}\,\varphi(y)\,ds(y),\quad x\in\partial D. \tag{40}$$

In our numerical implementations, we shall employ a scheme of the form (34), which is derived based on (40), to discretize T.

(ii) The adjoint T^* is exactly the incoming-to-outgoing (ItO) operator, that is, $T^*(\tilde{p}^s|_{\partial D})=p^s|_{\partial D}$ where p^s and $\tilde{p}^s$ are given in (36) and (37), respectively. In fact, by (39) we have

$$T^*(\tilde{p}^s|_{\partial D})=(\frac{1}{2}\mathbf{I}+\mathcal{D}^*)^{-1}(\frac{1}{2}\mathbf{I}+\mathcal{D})(\frac{1}{2}\mathbf{I}+\mathcal{D}^*)\varphi.$$

Applying the commutative property $\mathcal{D}^*\mathcal{D}=\mathcal{D}\mathcal{D}^*$, we find

$$T^*(\tilde{p}^s|_{\partial D}) \;=\; (\frac{1}{2}\mathbf{I}+\mathcal{D}^*)^{-1}(\frac{1}{2}\mathbf{I}+\mathcal{D}^*)(\frac{1}{2}\mathbf{I}+\mathcal{D})\varphi=(\frac{1}{2}\mathbf{I}+\mathcal{D})\varphi=p^s|_{\partial D}.$$

Notice that this implies that T is unitary, i.e., $TT^*=T^*T=\mathbf{I}$.

For notation clarity, we denote by T_x and T_y the outgoing-to-incoming operator T acting on functions of variables x and y, respectively. Below we show the symmetry of $T_x p^s(x,y)|_{\partial D}$ when the measurement surface is a sphere.

Lemma 3.8. *Assume that* $\partial D=\Gamma_{R_1}:=\{x\in\mathbb{R}^3:|x|=R_1\}$ *for some* $R_1>0$. *Then*

$$T_x p^s(x,y)=T_y p^s(y,x)\quad \textit{for all}\quad x,y\in\Gamma_{R_1}. \tag{41}$$

Proof. Noting that $p^s(x,y)$ fulfills the outgoing Sommerfeld radiation condition (8) with respect to both x and y, we can expand $p^s(x,y)$ into the convergent series

$$p^s(x,y)=\sum_{n=0}^{\infty}\sum_{m=-n}^{n} h_n^{(1)}(k|x|)Y_n^m(\hat{x})\sum_{n'=0}^{\infty}\sum_{m'=-n'}^{n'} h_{n'}^{(1)}(k|y|)Y_{n'}^{m'}(\hat{y})\,C_{n,m,n',m'},\quad C_{n,m,n',m'}\in\mathbb{C}$$

for all $|x|,|y|\geq R_1$. Since $p^s(x,y)=p^s(y,x)$ (see Lemma 5.1 in the Appendix), there holds the relation $C_{n,m,n',m'}=C_{n',m',n,m}$ for all $n,n'\in\mathbb{N}_0$, $m=-n,\cdots,n$ and $m'=-n',\cdots,n'$. By the definition of T_x and T_y, it is easy to deduce that

$$\begin{aligned}
T_x[p^s(x,y)|_{x,y\in\Gamma_{R_1}}] &= \sum_{n=0}^{\infty}\sum_{m=-n}^{n}\overline{h_n^{(1)}(kR)}Y_n^m(\hat{x})\sum_{n'=0}^{\infty}\sum_{m'=-n'}^{n'} h_{n'}^{(1)}(kR)Y_{n'}^{m'}(\hat{y})\,C_{n,m,n',m'},\\
T_y[p^s(x,y)|_{x,y\in\Gamma_{R_1}}] &= \sum_{n=0}^{\infty}\sum_{m=-n}^{n} h_n^{(1)}(kR)Y_n^m(\hat{x})\sum_{n'=0}^{\infty}\sum_{m'=-n'}^{n'}\overline{h_{n'}^{(1)}(kR)}Y_{n'}^{m'}(\hat{y})\,C_{n,m,n',m'}.
\end{aligned}$$

Changing x and y in the form of $T_y[p^s(x,y)|_{x,y\in\Gamma_{R_1}}]$ and using the relation $C_{n,m,n',m'}=C_{n',m',n,m}$, we obtain $T_x p^s(x,y)=T_y p^s(y,x)$ for all $x,y\in\{x:|x|=R_1\}$. □

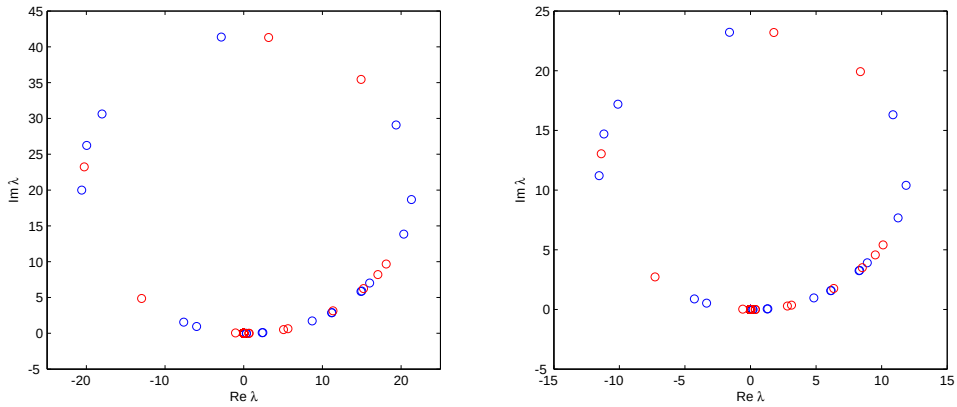

(a) $R_1 = 3$ (b) $R_1 = 4$

Figure 3: The distribution of eigenvalues of TN for different obstacles (red: apple-shaped; blue: peanut-shaped) in $2D$. The measurement curve $\partial D = \Gamma_{R_1}$ is circular.

Kirsch and Ruiz have shown in [12] that the far-field operator F (incited by plane waves) is normal and the scattering operator $\mathcal{S} := I + \frac{ik}{8\pi^2}F$ is unitary. This gives rise to the coincidence of the ranges of $(F^*F)^{1/4}$ and the corresponding far-field solution operator. Unfortunately, we do not know whether or not analogous properties could apply to TN and the near-field scattering operator $I + ic\,(TN)$ for some $c \in \mathbb{R}$. A further investigation of these operators could help mathematically justify the near-field version of the Linear Sampling Method [16] in a rigorous way. Our numerics show that the eigenvalues of TN all lie on the upper half of the complex plane; see Figures 3 and 4. In particular, the eigenvalues are located on a circle with the radius possibly depending on R_1, if the measurement curve $\partial D = \Gamma_{R_1}$ is circular; see Figure 3. We hope that Lemma 3.8, which is valid for spherical measurement surfaces only, could be useful in evaluating TN and the scattering operator in the near-field case. Recently, the product operator TN has been used in [7] for determining the Dirichlet eigenvalues of the region occupied by a sound-soft obstacle from near-field measurements.

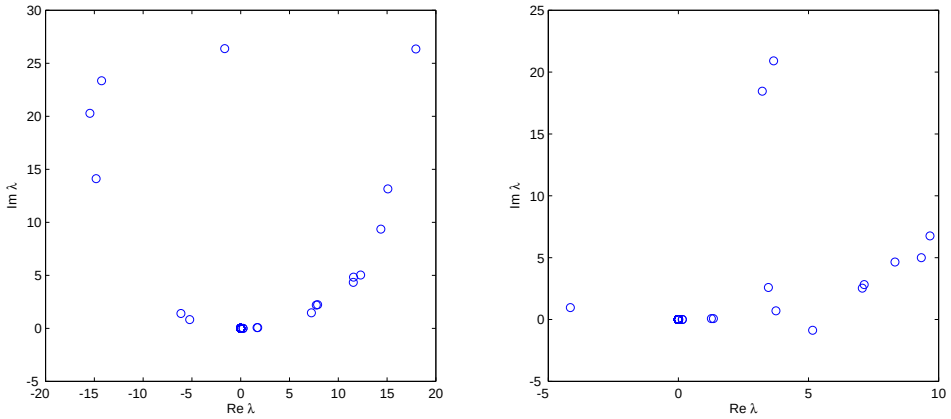

(a) Peanut-shaped, ellipse (b) Rounded-triangle-shaped, square

Figure 4: The distribution of eigenvalues of TN for peanut-shaped and rounded-triangle-shaped obstacles with non-circular measurement curves. The near-field data are measured on an ellipse (Left) and a square (Right), respectively.

3.4 Factorization of TN

We multiply the near-field operator N with the OtI operator T and then derive a factorization of the product operator TN. Our scheme relies on a refinement of the argument in the far-field case [12] in combination with the concept of the OtI operator introduced in Section 3.3 above.

We first introduce the incidence operator $H : L^2(\partial D) \to H^{1/2}(\Gamma)$ as

$$(Hg)(x) = \int_{\partial D} \Phi_k(x,y) g(y) ds(y) \quad \text{for} \quad x \in \Gamma. \tag{42}$$

The operator H is the restriction to Γ of a superposition of incident point source waves. It easily follows that $N = GH$, since $\Lambda(Hg) = \partial_\nu(Hg)$ on Γ for any $g \in L^2(\partial D)$. For $\varphi \in H^{-1/2}(\Gamma)$, recall the single-layer potential defined by

$$(S_k\varphi)(x) = \int_\Gamma \Phi_k(x,y)\, \varphi(y) ds(y), \quad x \in \mathbb{R}^3.$$

Let (u, v) be the unique solution of the problem (18)-(21) with $f = \partial_\nu (S_k\varphi)^+$ and $g = -\nu(S_k\varphi)^+$, that is,

$$\begin{aligned}
\Delta^* u + \rho\omega^2 u &= 0 && \text{in} \quad \Omega, && (43)\\
\Delta v + k^2 v &= 0 && \text{in} \quad \Omega, && (44)\\
\eta u \cdot \nu - \partial_\nu v &= \partial_\nu (S_k\varphi)^+ && \text{on} \quad \Gamma, && (45)\\
\mathbf{T}\, u + \nu v &= -\nu (S_k\varphi)^+ && \text{on} \quad \Gamma. && (46)
\end{aligned}$$

The operator $J : H^{-1/2}(\Gamma) \to H^{1/2}(\Gamma)$ is defined as $J\varphi := v|_\Gamma$ for $\varphi \in H^{-1/2}(\Gamma)$. Since the function $(S_k\varphi)(\cdot)$ satisfies the Helmholtz equation and the Sommerfeld radiation condition in Ω^c, rearranging the

terms in (43)-(46) yields

$$\begin{aligned} \Delta^* u + \rho\omega^2 u &= 0 \quad \text{in} \quad \Omega, && (47)\\ (\Delta + k^2)\,(S_k\varphi) &= 0 \quad \text{in} \quad \Omega^c, && (48)\\ \eta u\cdot\nu - \partial_\nu (S_k\varphi)^+ &= \Lambda v \quad \text{on} \quad \Gamma, && (49)\\ \mathbf{T}\, u + \nu\,(S_k\varphi)^+ &= -\nu v \quad \text{on} \quad \Gamma. && (50) \end{aligned}$$

This implies that $(u, S_k\varphi)$ is the unique solution to the problem (14)-(17) with $h = v|_\Gamma$. Therefore, we deduce from the definition of G and J that

$$(GJ\varphi)(x) = (S_k\varphi)|_{\partial D} = \int_\Gamma \Phi_k(x,y)\varphi(y)ds(y), \qquad x \in \partial D. \tag{51}$$

On the other hand, the adjoint operator $H^* : H^{-1/2}(\Gamma) \to L^2(\partial D)$ is given by

$$(H^*\varphi)(x) = \int_\Gamma \overline{\Phi_k(x,y)}\,\varphi(y)\,ds(y) \quad \text{for} \quad x \in \partial D. \tag{52}$$

Comparing the previous two identities and applying the outgoing-to-incoming operator yield the relation $H^* = TGJ$ (cf. (40)), implying that $H = J^*G^*T^*$. Hence, we get a factorization of the near-field operator multiplied by T as follows:

$$TN = TGH = \mathbb{G}J^*\mathbb{G}^*, \qquad \mathbb{G} := TG. \tag{53}$$

The form (53) will be used in the next section for the purpose of finding Ω from the data.

3.5 Inversion algorithm

In this subsection, we construct the characteristic function of the scatterer Ω in term of the spectral system of TN relying on the factorization form (53). We first show properties of the modified solution operator $\mathbb{G}$.

Lemma 3.9. *The operator $\mathbb{G} : H^{1/2}(\Gamma) \to L^2(\partial D)$ is compact with a dense range in $L^2(\partial D)$.*

Proof. The operator $\mathbb{G} = TG$ is compact since G is compact from $H^{1/2}(\Gamma)$ into $L^2(\partial D)$ and T is bounded from $L^2(\partial D)$ into $L^2(\partial D)$. The denseness of Range$(\mathbb{G})$ follows from the denseness of $G : H^{1/2}(\Gamma) \to L^2(\partial D)$ and that of $T : L^2(\partial D) \to L^2(\partial D)$; see Lemma 3.4 and Lemma 3.6 (ii). □

Below we show that Range$(\mathbb{G})$ can be utilized to characterize the domain Ω.

Lemma 3.10. *Let $\phi_z(\cdot) = \overline{\Phi_k(\cdot,z)}|_{\partial D}$ for $z \in B_R$. Then $z \in \Omega$ if and only if $\phi_z \in$ Range$(\mathbb{G})$.*

Proof. We first assume that $z \in \Omega$. Let (u, w) be the solution of the problem (18)-(21) with

$$f = (\partial_\nu \Phi_k(\cdot,z))|_\Gamma \in H^{-1/2}(\Gamma), \quad g = -\nu\Phi_k(\cdot,z) \in H^{1/2}(\Gamma)^3.$$

Then by the definition of Λ we see $\Lambda(w|_\Gamma) = (\partial_\nu w)|_\Gamma$. Hence the solution $(u, \Phi_k(\cdot,z))$ solves problem (14)-(17) with $h = w|_\Gamma$. From the definition of $\mathbb{G}$ and Lemma 3.6 (i) it follows that

$$\mathbb{G}\,h = T(G\,h) = T(\Phi(\cdot,z)|_{\partial D}) = \overline{\Phi(\cdot,z)}|_{\partial D}.$$

This implies that $\phi_z \in \text{Range}(\mathbb{G})$.

On the other hand, let $z \in B_R$ and assume that $\mathbb{G}h = \phi_z$ for some $h \in H^{1/2}(\Gamma)$, that is, $T(Gh) = \overline{\Phi_k(\cdot, z)}|_{\partial D}$. This implies that $Gh = \Phi_k(\cdot, z)|_{\partial D}$. Let p^s be the unique solution of the problem (14)-(17) with the same h. By uniqueness of outgoing solutions to the Dirichlet boundary value problem in $D^c := \mathbb{R}^3 \backslash \overline{D}$ and the analytic continuation, we get $p^s = \Phi_k(\cdot, z)$ in $\Omega^c \backslash \{z\}$. If $z \in B_R \backslash \overline{\Omega}$, the boundedness of $\lim_{x \to z} p^s(x)$ contradicts the singularity of $\Phi_k(x, z)$ at $x = z$. If $z \in \Gamma$, the trace regularity $p^s|_\Gamma \in H^{1/2}(\Gamma)$ is a contradiction to the fact that $\Phi_k(\cdot, z)|_\Gamma \notin H^{1/2}(\Gamma)$. Hence, we have $z \in \Omega$, which proves the lemma. □

Next we briefly review properties of the middle operator J in Lemma 3.11 below. The proof of Lemma 3.11 (ii) and (iii) is exactly the same with that contained in [12] but modified to be applicable to the new definition of J used in this paper.

Lemma 3.11. *Assume that k^2 is not a Dirichlet eigenvalue of $-\Delta$ in Ω and that ω is neither a Jones frequency nor an interior transmission eigenvalue. Then*

(i) *The operator $J : H^{-1/2}(\Gamma) \to H^{1/2}(\Gamma)$ is injective.*

(ii) *There exists a self-adjoint and coercive operator $J_0 : H^{-1/2}(\Gamma) \to H^{1/2}(\Gamma)$ such that $J - J_0 : H^{-1/2}(\Gamma) \to H^{1/2}(\Gamma)$ is compact.*

(iii) *Im $\langle \varphi, J\varphi \rangle > 0$ for all $\varphi \in H^{-1/2}(\Gamma)$ with $\varphi \neq 0$.*

Proof. (i) Assume that $J\varphi = v|_\Gamma = 0$, where (u, v) is the solution of the problem (43)-(46). Since k^2 is not a Dirichlet eigenvalue of $-\Delta$ in Ω, v vanishes identically in Ω and, in particular, $\partial v / \partial \nu = 0$ on Γ. Therefore, the solution pair $(u, S_k\varphi|_{\Omega^e})$ solves the homogeneous problem (14)-(17) with $h = 0$, implying that $u \equiv 0$ in Ω and $S_k\varphi \equiv 0$ in Ω^c. In particular, we get $(S_k\varphi)^+ = 0$ on Γ. Again using the assumption on k^2, we get $\varphi = 0$ on Γ since the single-layer boundary operator is an isomorphism from $H^{-1/2}(\Gamma)$ onto $H^{1/2}(\Gamma)$. Hence J is injective.

(ii) Define $J_0 : H^{-1/2}(\Gamma) \to H^{1/2}(\Gamma)$ by $J_0\varphi = v_1|_\Gamma$, where v_1 is the unique solution of the Neumann problem

$$\Delta v_1 - v_1 = 0 \quad \text{in} \quad \Omega, \qquad \partial_\nu v_1 = -\partial_\nu (S_i\varphi)^+ \quad \text{on} \quad \Gamma.$$

Setting $p_0 = S_i\varphi|_\Omega + v_1$ and applying the jump relation for single-layer potentials, we have

$$\Delta p_0 - p_0 = 0 \quad \text{in} \quad \Omega, \qquad \partial_\nu p_0 = \varphi \quad \text{on} \quad \Gamma.$$

By definition, $J_0\varphi = (p_0 - S_i\varphi)|_\Gamma$. We refer to [12, Theorem 2.4] for the proof of the coercivity of J_0. To investigate the compactness of $J - J_0$, we simplify the arguments employed in the proof of [12, Theorem 2.4]. Setting $v_2 = v - v_1$, we have $(J - J_0)\varphi = v_2|_\Gamma$, where $(u, v_2) \in H^1(\Omega)^3 \times H^1(\Omega)$ satisfies the inhomogeneous boundary value problem

$$\begin{aligned} \Delta^* u + \rho\omega^2 u = 0, \quad \Delta v_2 + k^2 v_2 = f \quad \text{in} \quad \Omega, \\ \eta u \cdot \nu - \partial_\nu v_2 = g, \quad \mathbf{T} u + \nu v_2 = h \quad \text{on} \quad \Gamma, \end{aligned} \tag{54}$$

with $(f, g, h) := (-(1 + k^2)v_1, \partial_\nu[(S_k - S_i)\varphi]^+, -\nu((S_k\varphi)^+ + p_0 - (S_i\varphi)^-)) \in H^1(\Omega) \times L^2(\Gamma) \times H^{1/2}(\Gamma)^3$ compactly embedding into $L^2(\Omega) \times H^{-1/2}(\Gamma) \times H^{-1/2}(\Gamma)^2$ for all $\varphi \in H^{-1/2}(\Gamma)$. Since

ω is not an interior transmission eigenvalue, the problem (54) is well-posed with the data $(f, g, h) \in L^2(\Omega) \times H^{-1/2}(\Gamma) \times H^{-1/2}(\Gamma)^2$. This implies that $J - J_0$ is compact from $H^{-1/2}(\Gamma)$ into $H^{1/2}(\Gamma)$.

(iii) Letting $w = v + S_k\varphi|_\Omega$, we have $J\varphi = v|_\Gamma = (w - S_k\varphi)|_\Gamma$. Moreover, (u, w) satisfies the problem

$$\begin{aligned} \Delta^* u + \rho\omega^2 u = 0, \quad \Delta w + k^2 w = 0 \quad \text{in} \quad \Omega, \\ \eta u \cdot \nu - \partial_\nu w = -\varphi, \quad \mathbf{T}\, u + \nu w = 0 \quad \text{on} \quad \Gamma. \end{aligned}$$

The coercivity of J then follows from [12, Theorem 2.3]. □

Thanks to the properties of the solution operator $\mathbb{G}$ and the operator J (see Lemmas 3.10 and 3.11), we may directly apply the following range identity (see [11, Theorem 2.15]) to the factorization form established in (53). Recall that the real and imaginary parts of an operator H over a Hilbert space are given by

$$\mathsf{Re}\, H := (H + H^*)/2, \quad \mathsf{Im}\, H := (H - H^*)/(2i).$$

Obviously, both ReH and ImH are self-adjoint operators.

Lemma 3.12 (**Range Identity**). *Let $X \subset Y \subset X^*$ be a Gelfand triple with Hilbert space Y and reflexive Banach space X such that the embedding is dense. Furthermore, let Y be a second Hilbert space and let $F : Y \to Y$, $G : X \to Y$ and $T : X^* \to X$ be linear and bounded operators with $F = GTG^*$. Assume further that*

(a) *G is compact with dense range.*

(b) *There exists $t \in [0, 2\pi]$ such that Re$[\exp(it)T]$ has the form Re$[\exp(it)T] = T_0 + T_1$ with some compact operator T_1 and some coercive operator $T_0 : X^* \to X$, that is, there exists $c > 0$ with*

$$\langle \varphi, T_0\varphi \rangle \geq c\|\varphi\|^2 \quad \text{for all} \quad \varphi \in X^*. \tag{55}$$

(c) *ImT is non-negative on Range$(G^*) \subset X^*$, that is, $\langle \varphi, (\mathsf{Im}\, T)\varphi \rangle \geq 0$ for all $\varphi \in$ Range(G^*).*

(d) *Re$[\exp(it)T]$ is one-to-one or ImT is strictly positive on the closure $\overline{\text{Range}(G^*)}$ of Range(G^*), that is, for all $\varphi \in \overline{\text{Range}(G^*)}$ with $\varphi \neq 0$ it holds that $\langle \varphi, (\mathsf{Im}\, T)\varphi \rangle > 0$.*

Then the operator $F_\sharp := |\mathsf{Re}\,[\exp(it)F]| + |\mathsf{Im}\, F|$ is positive definite and the ranges of $G : X \to Y$ and $F_\sharp^{1/2} : Y \to Y$ coincide.

To apply Lemma 3.12, we set

$$\begin{gathered} t = 0,\ F = TN,\ G = \mathbb{G},\ T = J^*,\ T_0 = J_0,\ T_1 = \mathsf{Re}\,(J - J_0), \\ Y = L^2(\partial D),\ \ X = H^{1/2}(\Gamma). \end{gathered}$$

In our settings, all the conditions in Lemma 3.12 are satisfied. In fact, conditions (a) and (b) follow from Lemma 3.9 and Lemma 3.11 (ii), respectively. Conditions (c) and (d) are guaranteed by Lemma 3.11 (iii). Combining Lemmas 3.12 and 3.10, we have the following result.

Theorem 3.13. *Let $z \in B_R$ and ϕ_z be defined in Lemma 3.10. Then $\phi_z(x)$ belongs to the range of $(TN)_\sharp$ if and only if $z \in \Omega$. Consequently, the near-field data $p^s(x,z)$ for all $x, z \in \partial D$ uniquely determine the interface Γ.*

As a consequence of Picard's range criterion we obtain the following sufficient and necessary computational criterion for precisely characterizing Ω through the eigensystem of TN.

Theorem 3.14. *Let $z \in B_R$ and let ϕ_z be defined in Lemma 3.10. Denote by $\lambda_j \in \mathbb{C}$ the eigenvalues of the operator TN with the corresponding normalized eigenfunctions $\psi_j \in L^2(\partial D)$. Then*

$$z \in \Omega \quad \Longleftrightarrow \quad W(z) := \left[\sum_{j=1}^{\infty} \frac{|\langle \phi_z, \psi_j \rangle_{L^2(\partial D)}|^2}{|\lambda_j|} \right]^{-1} > 0. \tag{56}$$

Thus, the function $W(z)$ on the right hand side of (56) can be regarded as the characteristic function for the domain occupied by the unknown scatterer Ω. By Theorem 3.14, the values of the indicator function $W(z)$ are positive for $z \in \Omega$ and zero for $z \in B_R \backslash \overline{\Omega}$. Numerically, the values of the indicator function inside the scatterer should be relatively larger than those outside. This will be confirmed in our 2D numerical examples presented in Section 4, where a rectangular domain containing Ω has been used in place of a circular domain of radius $R > 0$. However, it can be observed that the large values of the indicator function are at different scales. For example, they are oscillating in Figures 6 and 7. This may be due to the co-existence of compressional and shear waves incited insider the elastic body in comparison with earlier studies for pure compressional waves [5].

Remark 3.15. The indicator function (56) can be implemented even if limited aperture data are available on a sub-domain $S_D \subset \partial D$, i.e., the receivers and incident point sources are both located on S_D rather than the entire closed surface ∂D. In particular, S_D is allowed to be part of a plane in three dimensions or a line segment in two dimensions. We refer to Section 4.3 for the numerical examples.

4 Numerical experiments

In this section, we present numerical examples in two dimensions for testing accuracy and validity of the developed inversion scheme.

4.1 Discretization schemes

We first discuss how to discretize the outgoing-to-incoming mapping T in two dimensions, based on (40) and Fourier analysis. Employing the polar coordinates enables us to write

$$\partial D = \{x = \hat{x}\, \gamma_0(\theta_x) : \hat{x} = (\cos\theta_x, \sin\theta_x), \theta_x \in [0, 2\pi)\}.$$

For $g \in L^2(\partial D)$ and $\varphi \in L^2(\mathbb{S}^1)$, define

$$\tilde{g}(\hat{x}) := g(\hat{x}\, \gamma_0(\hat{x})) \in L^2(\mathbb{S}^1), \qquad \varphi(x) := \tilde{\varphi}(x/|x|) \in L^2(\partial D).$$

Then $g \in L^2(\partial D)$ if and only if $\tilde{g} \in L^2(\mathbb{S}^1)$. For each $g \in L^2(\partial D)$ we have the expansion

$$g(x) = \sum_{n=0}^{\infty} g_n \, e^{in\theta_x}, \qquad x \in \partial D$$

with

$$g_n := \int_{\mathbb{S}^1} \tilde{g}(\hat{x}) \, e^{-in\theta_x} \, ds(\hat{x}) = \int_{\partial D} g(x) \, e^{-in\theta_x} \Big/ \sqrt{[\gamma_0(\theta_x)]^2 + [\gamma_0'(\theta_x)]^2} \, ds(x). \tag{57}$$

Introduce the operator $F_D : L^2(\partial D) \to l^2$ by

$$F_D g = \mathbf{g}, \quad \mathbf{g} := \{g_n : n \in \mathbb{N}_0\} \in l^2. \tag{58}$$

Conversely, for $\mathbf{g} \in l^2$ define the operator $F_D^{-1} : l^2 \to L^2(\partial D)$ by

$$(F_D^{-1}\mathbf{g})(x) := g(x) = \sum_{n=0}^{\infty} g_n \, e^{in\theta_x}, \qquad x \in \partial D. \tag{59}$$

Further, it can be readily deduced from (58) and (59) that

$$F_D F_D^{-1} = I_{l^2}, \quad F_D^{-1} F_D = I_{L^2(\partial D)}. \tag{60}$$

Now we define the operators $G_D : H^{1/2}(\Gamma) \to l^2$, $H_D : l^2 \to H^{1/2}(\Gamma)$ and $T_D : l^2 \to l^2$ by

$$G_D := F_D G, \quad H_D := H F_D^*, \quad T_D = F_D T F_D^{-1},$$

respectively. Then the relation $TGJ = H^*$ implies that $T_D G_D J = H_D^*$. Recall the two-dimensional fundamental solution to the Helmholtz equation

$$\Phi_k(x, y) = \frac{i}{4} H_0^{(1)}(k|x - y|), \quad x \neq y.$$

For $|x| > |y|$ there holds the addition theorem (see [1, Chapter 3.4]):

$$\Phi_k(x, y) = \frac{i}{4} \sum_{n=-\infty}^{+\infty} H_n^{(1)}(k|x|) \, J_n(k|y|) \, e^{in(\theta_x - \theta_y)}.$$

Here J_n are known as Bessel functions of order n and $H_n^{(1)}$ Hankel functions of the first kind of order n. Hence, for $x \in \partial D$,

$$(H_D^* \psi)(x) = (F_D H^* \psi)(x) = F_D \left(\int_\Gamma \overline{\Phi(x, y)} \psi(y) \, ds(y) \right) = \left\{ \sum_{m=-\infty}^{\infty} A_{n,m} \Psi_m : n \in \mathbb{N} \right\},$$

$$(G_D J \psi)(x) = (F_D G J \psi)(x) = F_D \left(\int_\Gamma \Phi(x, y) \psi(y) \, ds(y) \right) = \left\{ \sum_{m=-\infty}^{\infty} B_{n,m} \Psi_m : n \in \mathbb{N} \right\},$$

where

$$\begin{aligned} \Psi_m &= \int_\Gamma J_m(k|y|) \, e^{-im\theta_y} \psi(y) \, ds_y, \\ A_{n,m} &= -\frac{i}{4} \int_0^{2\pi} \overline{H_m^{(1)}(k \, \gamma_0(\theta_x))} \, e^{i(m-n)\theta_x} \, d\theta_x, \\ B_{n,m} &= \frac{i}{4} \int_0^{2\pi} H_m^{(1)}(k \, \gamma_0(\theta_x)) \, e^{i(m-n)\theta_x} \, d\theta_x. \end{aligned} \tag{61}$$

Now we truncate the series in each entry of $H_D^*\psi$ and $G_D J\psi$ to get an approximation of T_D: $T_D \approx \mathbf{A}\mathbf{B}^{-1}$ where for some $M_1 > 0$,

$$\mathbf{A} = \begin{bmatrix} A_{-M_1,-M_1} & A_{-M_1,-M_1+1} & \cdots & A_{-M_1,M_1} \\ A_{-M_1+1,-M_1} & A_{-M_1+1,-M_1+1} & \cdots & A_{-M_1,M_1} \\ \vdots & \vdots & \ddots & \vdots \\ A_{M_1,-M_1} & A_{M_1,-M_1+1} & \cdots & A_{M_1,M_1} \end{bmatrix},$$

$$\mathbf{B} = \begin{bmatrix} B_{-M_1,-M_1} & B_{-M_1,-M_1+1} & \cdots & B_{-M_1,M_1} \\ B_{-M_1+1,-M_1} & B_{-M_1+1,-M_1+1} & \cdots & B_{-M_1,M_1} \\ \vdots & \vdots & \ddots & \vdots \\ B_{M_1,-M_1} & B_{M_1,-M_1+1} & \cdots & B_{M_1,M_1} \end{bmatrix}.$$

Here $[\cdot]_{i,j}$ represent the rectangular Cartesian components of a square matrix. Note that we have assumed that the matrix $\mathbf{B}$ is invertible for the chosen $M_1 > 0$. For $g \in L^2(\partial D)$, the outgoing-to-incoming operator T can be discretized by (cf. (57))

$$\begin{aligned} (Tg)(x) &= (F_D^{-1} T_D F_D g)(x) \\ &\approx F_D^{-1} T_D \left\{ \int_{\partial D} g(y)\, e^{-im\theta_y} / \sqrt{[\gamma_0(\theta_y)]^2 + [\gamma_0'(\theta_y)]^2}\, ds(y) : |m| < M_1 \right\} \end{aligned}$$

Applying $T_D \approx \mathbf{A}\mathbf{B}^{-1}$ and using the definition of F_D, we obtain

$$(Tg)(x) \approx (T_{M_1} g)(x) := \int_{\partial D} K_{M_1}(x,y) g(y)\, ds_y,$$

where the truncated kernel K_{M_1} is defined by

$$K_{M_1}(x,y) = \sum_{n=-M_1}^{M_1} \sum_{m=-M_1}^{M_1} \left[\mathbf{A}\mathbf{B}^{-1}\right]_{n+M_1+1,m+M_1+1} e^{i(n\theta_x - m\theta_y)} / \sqrt{[\gamma_0(\theta_y)]^2 + [\gamma_0'(\theta_y)]^2}.$$

Remark 4.1. In the special case that ∂D is a sphere of radius R_1, i.e., $\gamma_0(\theta_x) \equiv R_1$ is independent of θ_x, only the diagonal elements of $\mathbf{A}$ and $\mathbf{B}$ remain, while the other off-diagonal terms vanish identically. The kernel K_{M_1} then reduces to the following simple form (cf. [5, Section 6]):

$$K_{M_1}(x,y) = -\frac{1}{R_1} \sum_{n=-M_1}^{M_1} \left(\frac{\overline{H_n^{(1)}(kR_1)}}{H_n^{(1)}(kR_1)} \right) e^{in(\theta_x - \theta_y)}.$$

To discretize the near-field operator N, we take the scattered field at a uniformly distributed grid over ∂D with the step size $\Delta\theta_x = \Delta\theta_y = 2\pi/M_2$ for some $M_2 \in \mathbb{N}$, that is,

$$\theta_x = \theta_x(j) = (j-1)\Delta\theta_x, \quad \theta_y = \theta_y(j) = (j-1)\Delta\theta_y, \quad j \in \mathcal{K},$$

where $\mathcal{K} := \{j \in \mathbb{N} : 1 \le j \le M_2\}$. Then we have the near-field matrix

$$\mathbf{N}_{M_2 \times M_2} = [p^s(\theta_x(p), r(\theta_x(p)); \theta_x(p), r(\theta_x(p)))]_{p,q \in \mathcal{K}},$$

and the finite-dimensional matrix $\mathbf{T}_{M_2\times M_2} = [K_{M_1}(\theta_x(p), r(\theta_x(p)); \theta_x(p), r(\theta_x(p)))]_{p,q\in\mathcal{K}}$ for T_{M_2}. Letting $\mathbf{N}^T_{M_2\times M_2} = \mathbf{T}_{M_2\times M_2}\mathbf{N}_{M_2\times M_2}$, we can approximate the characteristic function of W defined in Theorem 3.14 by the finite series

$$\widetilde{W}(z) := \left[\sum_{j=1}^{M_2} \frac{|(\phi_z, \psi_j)_{l^2}|^2}{|\lambda_j|}\right]^{-1} \quad \text{for} \quad z \in B_R, \tag{62}$$

where $\phi_z = \overline{\Phi(\cdot, z)}|_{\partial D}$ and $\{\psi_j, \lambda_j\}_{j=1}^{M_2}$ is an eigensystem of the matrix $\mathbf{N}^T_{M_2\times M_2,\#} := |\text{Re}\,(\mathbf{N}^T_{M_2\times M_2})| + |\text{Im}\,(\mathbf{N}^T_{M_2\times M_2})|$.

4.2 Inversion scheme by converting near-field data to far-field patterns

In contrast to the ïndirect"factorization of the near-field operator, the far-field operator $F : L^2(\mathbb{S}^2) \to L^2(\mathbb{S}^2)$, defined by

$$(Fg)(\hat{x}) = \int_{\mathbb{S}^2} v^\infty(\hat{x}, d)\, g(d)\, ds(d), \qquad \hat{x} \in \mathbb{S}^2,$$

can be factorized in a straightforward way (see [12]). Denote by $v^\infty(\hat{x}, d)$, $v^s(\hat{x}, d)$ and $v(x, d)$ the far-field pattern, scattered and total fields associated with the incident plane wave $p^{in} = e^{ikx\cdot d}$ of direction $d \in \mathbb{S}^2$, respectively. Hence, it is very natural to apply Kirsch's idea [11, Chapter 2.4] of converting the near-field data $\{p^s(x, z) : x, z \in \partial D\}$ into the far-field patterns $\{v^\infty(\hat{x}, d) : \hat{x}, d \in \mathbb{S}^2\}$. To achieve this, it is necessary to establish the mixed reciprocity relation $p^\infty(\hat{x}, z) = v^{sc}(z, -\hat{x})$, and then generalize [17, Theorem 4.15] for a sound-soft obstacle to the case of the fluid-solid interaction model. Since such an argument is standard, we omit the details and state the resulting scheme in the following.

Given $f \in H^{1/2}(\partial D)$, consider the boundary value problem of finding an outgoing Sommerfeld radiating wave $w \in H^1_{loc}(\mathbb{R}^3\backslash\overline{D})$ such that

$$\Delta w + k^2 w = 0 \quad \text{in} \quad \mathbb{R}^3\backslash\overline{D}, \quad w = f \quad \text{on} \quad \partial D. \tag{63}$$

The far-field pattern w^∞ of w defines the far-field solution operator $G_D^+ : H^{1/2}(\partial D) \to L^2(\mathbb{S}^2)$ by $G_D^+ f = w^\infty$. Introduce the operator $B : L^2(\mathbb{S}^2) \to L^2(\partial D)$ by

$$(Bg)(\xi) = \int_{\mathbb{S}^2} \partial_\nu[w(\xi, d) + e^{ik\xi\cdot d}]\, g(d)\, ds(d), \quad \xi \in \partial D, \tag{64}$$

where $w(\xi, d)$ is the solution of (63) with $f = -e^{ikx\cdot d}|_{\partial D}$. We have

Lemma 4.2. **(i)** *The far-field operator F can be factorized as $F = G_D^+ NB$.*

(ii) *Let $z \in B_R$ and $\varphi_z(\hat{x}) = e^{-ik\hat{x}\cdot z}$. Denote by $\lambda_j \in \mathbb{C}$ the eigenvalues of the operator $F_\# = (G_D^+ NBg)_\#$ with the corresponding normalized eigenfunctions $\phi_j \in L^2(\mathbb{S}^2)$. Then*

$$z \in \Omega \iff W_0(z) := \left[\sum_{j=1}^{\infty} \frac{|\langle\varphi_z, \psi_j\rangle_{L^2(\mathbb{S}^2)}|^2}{\lambda_j}\right]^{-1} > 0. \tag{65}$$

Implementing the above scheme requires an efficient forward solver for the boundary value problem (63). An analytical solution can be constructed only if $\partial D = \Gamma_{R_1}$ is a circle. In our numerical examples below, we apply such scheme to spherical measurement surfaces in 2D only. The truncated far-field matrix $\mathbf{F}_{M_2\times M_2}$ can be obtained following the process discussed in [17]. Consequently, the series in (65) can be approximated by

$$\widetilde{W}_0(z) := \left[\sum_{j=1}^{M_2} \frac{|(\tilde{\varphi}_z, \tilde{\psi}_j)_{l^2}|^2}{\tilde{\lambda}_j}\right]^{-1} \quad \text{for} \quad z \in B_R, \tag{66}$$

where $\tilde{\phi}_z(\hat{x}) = e^{-ikz\cdot(\cos\theta_x, \sin\theta_x)}$ and $\{\tilde{\psi}_j, \tilde{\lambda}_j\}_{j=1}^{M_2}$ is an eigensystem of the matrix $(\mathbf{F}_{M_2\times M_2})_{\#}$. It is expected that if M_2 is taken large enough, the series in (62) and (66) approximate the true values of W and W_0, respectively. Thus, $\widetilde{W}(z)$ and $\widetilde{W}_0(z)$ should be very small in $B_R\backslash\overline{\Omega}$ and considerably large in Ω.

4.3 Numerical examples

In the following experiments, we use (A1) and (A2) to represent the algorithms using the criteria (56) and (66), respectively. The direct problem is solved by using a finite element method in conjunction with a DtN map on an artificial boundary, and the near-field data is measured at 64 points with 64 source points equivalently distributed on ∂D, that is, $M_2 = 64$. In Figure 5 we show the four configurations of underlying elastic bodies to be reconstructed. We employ dotted lines to represent ∂D, i.e., the position where the near-field data are collected and where the incident sources are located. Unless otherwise stated, we always set $\omega = 3$, $\mu = 2$, $\lambda = 1$, $\rho_f = 1$, $\rho = 2$, $M_1 = 50$, and plot the map $\widetilde{W}_t(z), t = 0, 1$ against the sampling point z. We choose $k = 7, 5, 5, 2$ for peanut-shaped, kite-shaped, mix-shaped and rounded-triangle-shaped obstacles, respectively.

Example 1: We choose $\partial D = \Gamma_{R_1}$ to be a circle of radius R_1, and set $R_1 = 5$ for the kite-shaped obstacle (see Figure 5 (a)) and $R_1 = 6$ for the mix-shaped obstacle (see Figure 5 (b)). The reconstructions from unpolluted and polluted data using the algorithms (A1) and (A2) are presented in Figures 6 and 7, respectively. The near-field acoustic data are perturbed by the multiplication of $(1 + \delta\xi)$ with the noise level $\delta\%$, where ξ is an independent and uniformly distributed random variable generated between -1 and 1. We set $\delta = 0\%$ in Figures 6 and 7 (a) and (e), $\delta = 1\%$ in Figures 6 and 7 (b) and (f), $\delta = 2\%$ in Figures 6 and 7 (c) and (g) and $\delta = 5\%$ in Figures 6 and 7 (d) and (h), respectively. It turns out that the proposed inversion scheme using the outgoing-to-incoming operator is more stable than the scheme (A2) described in Section 4.2, especially at the low noise levels.

Example 2: In the second example, the measurement curve ∂D is chosen to be an ellipse with the semi-major axis $a = 4$ and semi-minor axis $b = 3$. The focal points are located at x-axis; see Figure 5 (c). We apply the algorithm (A1) proposed in this paper to reconstruct the peanut-shaped obstacle from unpolluted and polluted data; see Figures 8 (c), (d), (e) and (f).

In Figures 8 (a) and (b), we use limited aperture near-field data (unpolluted) to recover the boundary of the elastic body. The incident point sources and receivers are supposed to be uniformly located at

$$\begin{aligned}\Gamma^{(1)} : &= \{(a\cos\theta, b\sin\theta) : \theta \in (0, \pi/2)\} \quad \text{in Figure 8 (a)},\\ \Gamma^{(2)} : &= \{(a\cos\theta, b\sin\theta) : \theta \in (0, 3\pi/4)\} \quad \text{in Figure 8 (b)}.\end{aligned}$$

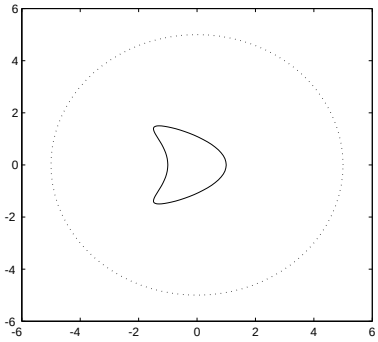

(a) Example 1, Kite-shaped

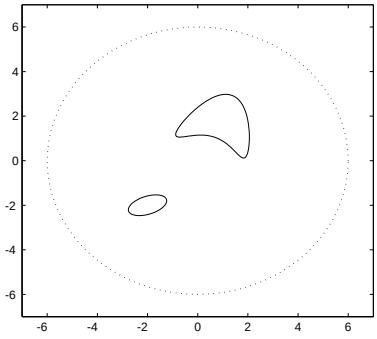

(b) Example 1, mix-shaped

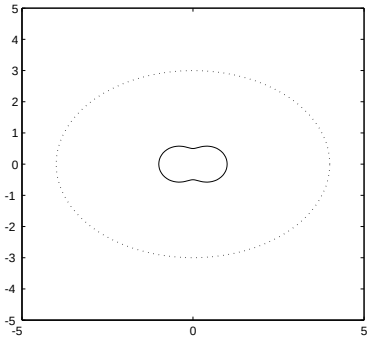

(c) Example 2, Peanut-shaped

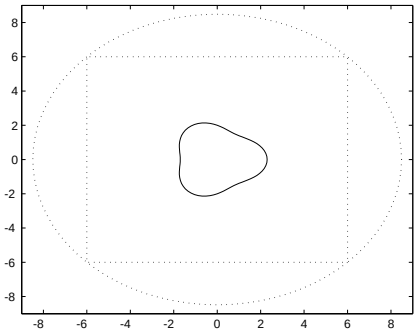

(d) Example 3, Rounded-triangle-shaped

Figure 5: The four configurations to be reconstructed. Solid line: Γ; dotted lines: ∂D. In Example 3, ∂D is allowed to be the line segments illustrated in (d).

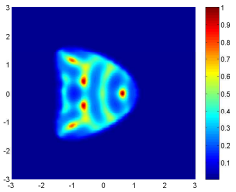

(a) (A1), no noise

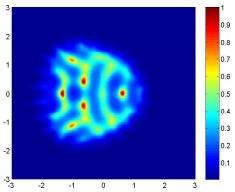

(b) (A1), 1% noise

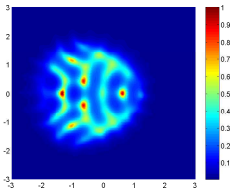

(c) (A1), 2% noise

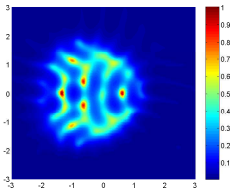

(d) (A1), 5% noise

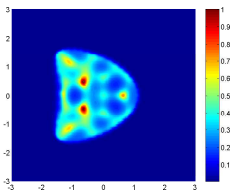

(e) (A2), no noise

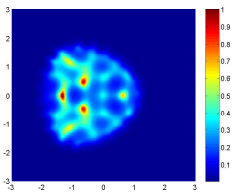

(f) (A2), 1% noise

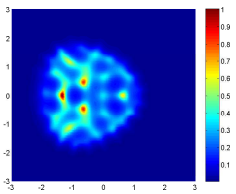

(g) (A2), 2% noise

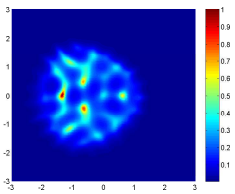

(h) (A2), 5% noise

Figure 6: Reconstruction of the kite-shaped obstacle with $\partial D = \{x \in \mathbb{R}^2 : |x| = 5\}$.

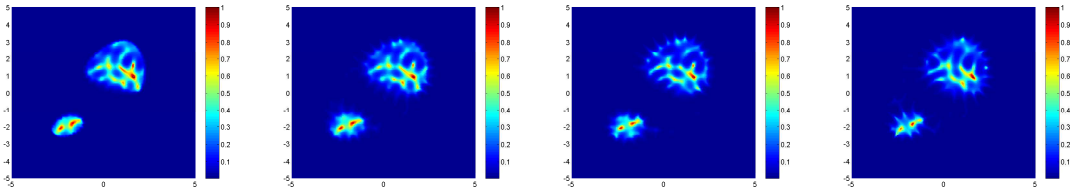

(a) (A1), no noise (b) (A1), 1% noise (c) (A1), 2% noise (d) (A1), 5% noise

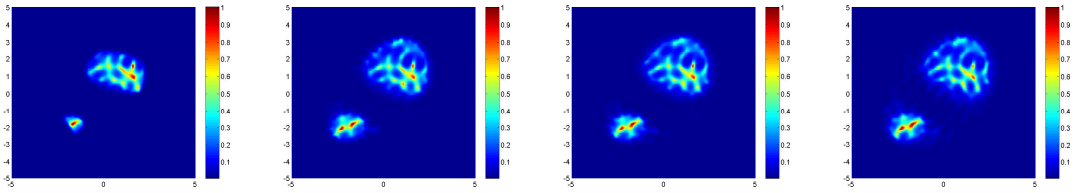

(e) (A2), no noise (f) (A2), 1% noise (g) (A2), 2% noise (h) (A2), 5% noise

Figure 7: Reconstruction of the mix-shaped obstacle with $\partial D = \{x \in \mathbb{R}^2 : |x| = 6\}$.

That is, the elastic body is illuminated by 32 and 48 point source waves, respectively. The positions where the near-field data are recorded coincide with the incident point sources, that is, the transmitters and receivers are placed on the same part of the near field measurement surface. In this case, the matrices **A** and **B** are still calculated using the geometry of the entire closed curve ∂D (see (61)), whereas the outgoing-to-incoming operator T is approximated only on the sub-domain $\Gamma^{(j)}$ of ∂D. Clearly, the reconstruction from the limited data is less reliable and precise compared to the full-data case.

Example 3: In the third example, we apply the algorithm (A1) to recover the rounded-triangle-shaped obstacle from limited data collected on a line segment l. We assume that l lies on the boundary of the square centered at the origin with side length $R_0 = 6$. We will show the reconstruction results associated with the following different line segments:

$$\begin{aligned} l_1 : &= \{(R_0/\tan(\pi/2-\theta), R_0) : \theta \in [\pi/4, 3\pi/4] =: \Theta_1\}, \\ l_2 : &= \{(-R_0, R_0/\tan(\pi-\theta)) : \theta \in [3\pi/4, 5\pi/4] =: \Theta_2\}, \\ l_3 : &= \{(R_0/\tan(\theta-3\pi/2), -R_0) : \theta \in [5\pi/4, 7\pi/4] =: \Theta_3]\}, \\ l_4 : &= \{(R_0, R_0/\tan\theta) : \theta \in [0, \pi/4] \cup [7\pi/4, 2\pi) =: \Theta_4\}. \end{aligned}$$

Since limited near-field data are available only, we can approximate the outgoing-to-incoming operator T on l_j by computing each entry of the matrix $\mathbf{AB}^{-1}$ on a closed curve S_{l_j} containing l_j, as done in Example 2. From numerical point of view it is natural and convenient to use circular curves as the extended part. Hence, we define the piecewise smooth curves

$$S_{l_j} := l_j \cup \{\sqrt{2}R_0(\cos\theta, \sin\theta) : \theta \in [0, 2\pi)\backslash\Theta_j\}.$$

We take $M_2 = 128$. The reconstruction results from the near-field measurement on S_{l_j} and l_j are presented in Figure 9 (a)-(d) and (e)-(h), respectively. It is concluded from Figure 9 (a)-(d) that the near-field imaging does not rely too much on the choice of the closed measurement curve, but varies with the directions of the measurement line segments. Obviously, the extension from l_j to S_{l_j} is not unique. However, our numerics show that the reconstruction is independent of the way of extending l_j to a closed

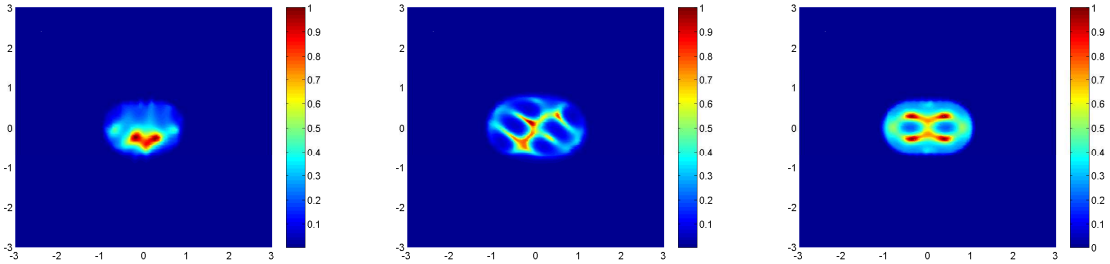

(a) 50%- data (b) 75%- data (c) Full-data

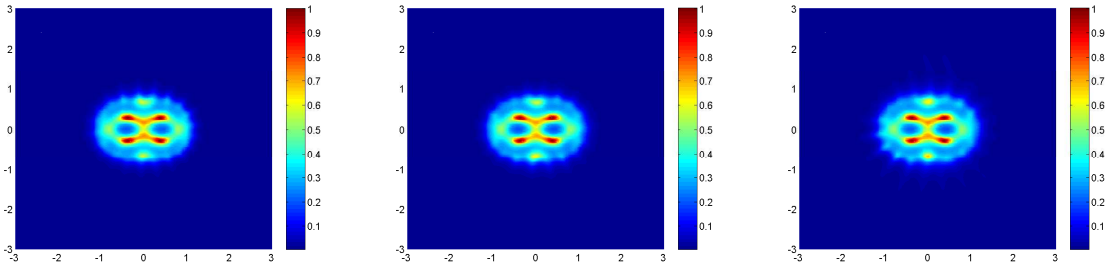

(d) 1% noise (e) 2% noise (f) 5% noise

Figure 8: Reconstruction of the peanut-shaped obstacle with $\partial D = \{(4\cos\theta, 3\sin\theta) : \theta \in [0, 2\pi)\}$ in (c)-(f). Limited aperture data from part of the ellipse are used in (a) and (b).

curve. To see this point, we reconstruct the elastic body from near-field measurement taken on $l_2 \cup l_3$, with the matrix $\mathbf{AB}^{-1}$ calculated on different closed curves $S^j \supseteq \{l_2 \cup l_3\}$, $j = 1, 2, 3, 4$, given by

$$\begin{aligned} S^1 : &= l_2 \cup l_3 \cup l_1 \cup \{\sqrt{2}R_0(\cos\theta, \sin\theta) : \theta \in [0, 2\pi)\backslash(\Theta_2 \cup \Theta_3 \cup \Theta_1)\}, \\ S^2 : &= l_2 \cup l_3 \cup l_4 \cup \{\sqrt{2}R_0(\cos\theta, \sin\theta) : \theta \in [0, 2\pi)\backslash(\Theta_2 \cup \Theta_3 \cup \Theta_4)\}, \\ S^3 : &= l_2 \cup l_3 \cup \{\sqrt{2}R_0(\cos\theta, \sin\theta) : \theta \in [0, 2\pi)\backslash(\Theta_2 \cup \Theta_3)\}, \\ S^4 : &= l_2 \cup l_3 \cup l_1 \cup l_4. \end{aligned}$$

It is seen from Figure 10 that the imaging results indeed do not depend on the choice of S^j. Finally, we illustrate in Figure 11 the reconstruction of the peanut-shaped obstacle from the near-field data measured on one or several line segments. Again the matrix $\mathbf{AB}^{-1}$ is computed by extending the measurement line segments with circular curves. Clearly, increasing observation line segments with different directions leads to a better imaging quality.

5 Appendix

Denote by $p^s(\cdot, z)$ the scattering solution to the problem (3)-(8) with the incident point source wave $\Phi_k(\cdot, z)$ for $z \in \mathbb{R}^3\backslash\overline{\Omega}$. We show the symmetry of $p^s(x, z)$ with respect to x and z, which has been used in the proof of Lemma 3.8.

Lemma 5.1. *The scattering solution to the problem (3)-(8) with an incident point source satisfies*

$$p^s(y, z) = p^s(z, y), \quad y, z \in \mathbb{R}^3\backslash\overline{\Omega}. \tag{67}$$

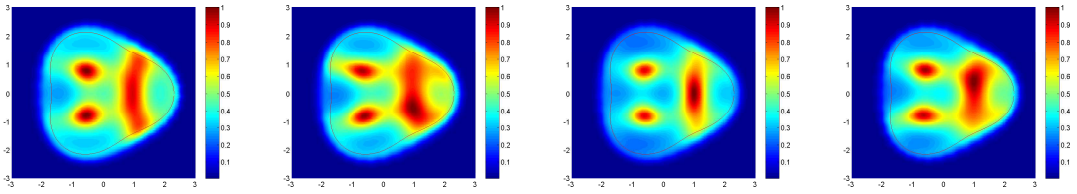

(a) S_{l_1} (b) S_{l_2} (c) S_{l_3} (d) S_{l_4}

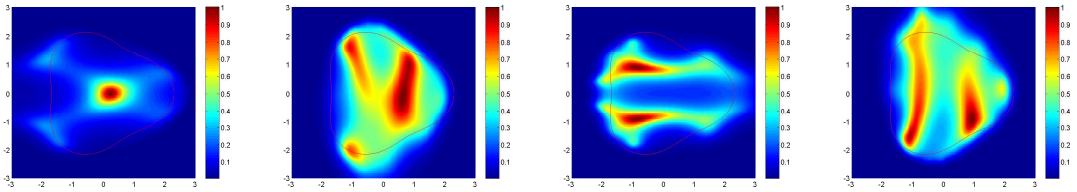

(e) l_1 (f) l_2 (g) l_3 (h) l_4

Figure 9: Reconstruction of the rounded-triangle-shaped obstacle from limited aperture data collected on the line segment l_j in (e)-(h), and from the full data measured on the closed curve S_{l_j} in (a)-(d).

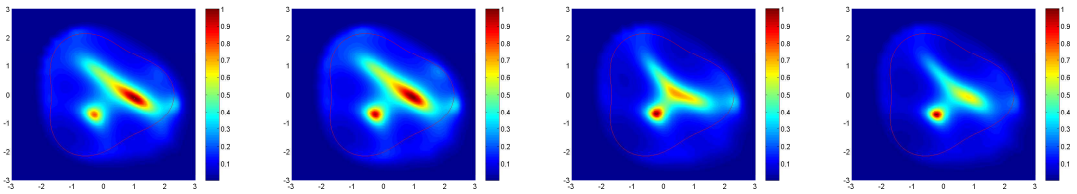

(a) S^1 (b) S^2 (c) S^3 (d) S^4

Figure 10: Reconstruction of the rounded-triangle-shaped obstacle from limited aperture data collected on $l_2 \cup l_3$. To compute the operator T, we calculate the matrix $\mathbf{AB}^{-1}$ using different closed curves S^j containing $l_2 \cup l_3$.

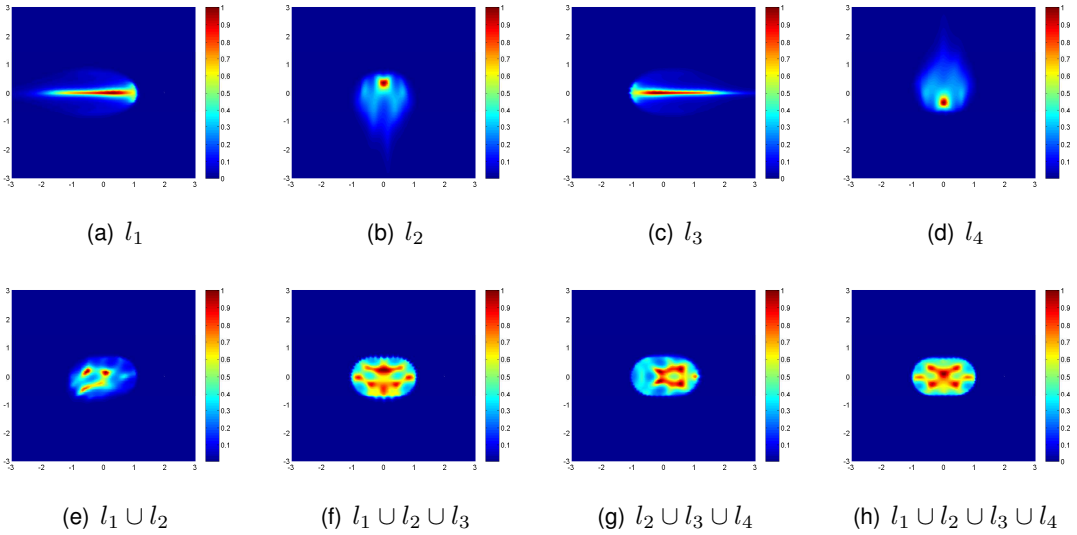

(a) l_1 (b) l_2 (c) l_3 (d) l_4

(e) $l_1 \cup l_2$ (f) $l_1 \cup l_2 \cup l_3$ (g) $l_2 \cup l_3 \cup l_4$ (h) $l_1 \cup l_2 \cup l_3 \cup l_4$

Figure 11: Reconstruction of the peanut-shaped obstacle from the near-field data measured on one or several line segments.

Proof. Choose $\epsilon > 0$ sufficiently small and $R > 0$ sufficiently large such that

$$\Omega \subset B_R, \quad B_\epsilon(z) \subset B_R \backslash \overline{\Omega}, \quad B_\epsilon(y) \subset B_R \backslash \overline{\Omega}, \quad B_\epsilon(y) \cap B_\epsilon(z) = \emptyset.$$

Applying Green's second formula to the total fields $p(x, y)$ and $p(x, z)$ in the region $B_R \backslash \{\overline{\Omega} \cup B_\epsilon(y) \cup B_\epsilon(z)\}$, we find

$$0 = \left(\int_{\partial B_R} - \int_{\partial B_\epsilon(z)} - \int_{\partial B_\epsilon(z)} - \int_\Gamma \right) \left[\partial_\nu p(x, y) p(x, z) - p(x, y) \partial_\nu p(x, z) \right] ds(x). \tag{68}$$

In view of the coupling conditions between p and u, we derive from Betti's formula that

$$\int_\Gamma \left[\partial_\nu p(x, y) p(x, z) - p(x, y) \partial_\nu p(x, z) \right] ds(x) = 0.$$

Letting $R \to \infty$ in (68) we get

$$\left(\int_{\partial B_\epsilon(z)} + \int_{\partial B_\epsilon(y)} \right) \left[\partial_\nu p(x, y) p(x, z) - p(x, y) \partial_\nu p(x, z) \right] ds(x) = 0, \tag{69}$$

since $p(x, y)$ and $p(x, z)$ are both outgoing radiating solutions. Applying Green's second theorem to $p(x, z)$ and $p^s(x, y)$ in the ball $B_\epsilon(y)$ yields

$$0 = \int_{\partial B_\epsilon(y)} \left[\partial_\nu p^s(x, y) p(x, z) - p^s(x, y) \partial_\nu p(x, z) \right] ds(x). \tag{70}$$

Analogously, there holds that

$$0 = \int_{\partial B_\epsilon(z)} \left[\partial_\nu p^s(x, z) p(x, y) - p^s(x, z) \partial_\nu p(x, y) \right] ds(x). \tag{71}$$

Inserting (70) and (71) into (69) and again applying Green's second theorem yield

$$\begin{aligned} 0 &= \int_{\partial B_\epsilon(z)} [\partial_\nu p(x,y)\Phi(x,z) - p(x,y)\partial_\nu \Phi_k(x,z)]\, ds(x) \\ &\quad + \int_{\partial B_\epsilon(y)} [\partial_\nu \Phi_k(x,y)p(x,z) - \Phi_k(x,y)\partial_\nu p(x,z)]\, ds(x) \\ &= p(z,y) - p(y,z). \end{aligned}$$

Since $\Phi_k(z,y) = \Phi_k(y,z)$, we obtain $p^s(z,y) = p^s(y,z)$. □

References

[1] D. Colton, and R. Kress, *Inverse Acoustic and Electromagnetic Scattering Theory*, Berlin, Springer, 1998.

[2] J. Elschner, G.C. Hsiao and A. Rathsfeld, An inverse problem for fluid-solid interaction, *Inverse Problems and Imaging* **2** (2008), 83–120.

[3] J. Elschner, G.C. Hsiao and A. Rathsfeld, An optimization method in inverse acoustic scattering by an elastic obstacle, *SIAM J. Appl. Math.* **70** (2009), 168–187.

[4] G.C. Hsiao, R.E. Kleinman and G.F. Roach, Weak solution of fluid-solid interaction problem, *Math. Nachr.* **218** (2000), 139–163.

[5] G. Hu, J. Yang, B. Zhang and H. Zhang, Near-field imaging of scattering obstacles via the factorization method, Inverse Problems 30 (2014) 095005.

[6] G. Hu, A. Kirsch and T. Yin, Factorization method in inverse interaction problems with bi-periodic interfaces between acoustic and elastic waves, *Inverse Problems and Imaging*, in press, 2015.

[7] A. Lechleiter and S. Peters, The inside-outside duality for inverse scattering problems with near field data, Inverse Problems 31 (2015), 085004.

[8] D.S. Jones, Low-frequency scattering in elasticity, *Q.J. Mech. Appl. Math.* **34** (1981) 431-451.

[9] D.S. Jones, Low-frequency scattering by a body in lubricated contact, *Quart. J. Mech. Appl. Math.* **36** (1983) 111-137.

[10] A. Kirsch, Characterization of the shape of a scattering obstacle using the spectral data of the far field operator, *Inverse Problems* **14** (1998), 1489–1512.

[11] A. Kirsch and N. Grinberg, *The Factorization Method for Inverse Problems*, New York, Oxford Univ. Press, 2008.

[12] A. Kirsch and A. Ruiz, The factorization method for an inverse fluid-solid interaction scattering problem, *Inverse Problems and Imaging* **6** (2012), 681–695.

[13] A. Kirsch, An integral equation for Maxwell's equations in a layered medium with an application to the factorization, *J. Integral Equ. Appl.* **(19)** (2007), 333–358.

[14] C.J. Luke and P.A. Martin, Fluid-solid interaction: Acoustic scattering by a smooth elastic obstacle, *SIAM J. Appl. Math.* **55** (1995), 904–922.

[15] P. Monk and V. Selgas, An inverse fluid-solid interaction problem, *Inverse Probl. Imaging* **3** (2009), 173–198.

[16] P. Monk and V. Selgas, Near field sampling type methods for the inverse fluid-solid interaction problem, *Inverse Problems and Imaging* **5** (2011), 465–483.

[17] M. Orispää, On point sources and near field measurements in invese acoustic obstacle scattering, Doctorial Thesis, University of Oulu, Finland, 2002.

[18] M. Sanna, Numerical simulation of fluid-structure interaction between acoustic and elastic waves, University of Jyväskylä, PhD Thesis, 2011.